# Recurrent emergence of carbapenem resistance in *Klebsiella pneumoniae* mediated by an inhibitory *ompK36* mRNA secondary structure

Authors: Joshua L. C. Wong† [1,2], Sophia David† [3], Julia Sanchez-Garrido[1], Jia Z. Woo[4],

Wen Wen Low[1], Fabio Morecchiato[5], Tommaso Giani[5,6], Gian Maria Rossolini[5,6],

Stephen J. Brett[2], Abigail Clements[1], David M Aanensen[3], Silvi Rouskin[4] and Gad

Frankel[1]


† These authors contributed equally to this work.


Affiliations:

1. Centre for Molecular Bacteriology and Infection, Department of Life Sciences, Imperial College London, London, United Kingdom.
2. Department of Surgery and Cancer, Section of Anaesthetics, Pain Medicine and Intensive Care, Imperial College London, London, United Kingdom.
3. Centre for Genomic Pathogen Surveillance, Big Data Institute, University of Oxford, United Kingdom.
4. Department of Microbiology, Harvard Medical School, Boston, MA, United States of America.
5. Department of Experimental and Clinical Medicine, University of Florence, Florence, Italy.
6. Clinical Microbiology and Virology Unit, Careggi University Hospital, Florence, Italy.

Corresponding author: Gad Frankel g.frankel@imperial.ac.uk

**Abstract**

Outer membrane porins in Gram-negative bacteria facilitate antibiotic influx. In *Klebsiella pneumoniae* (KP), modifications in the porin OmpK36 are implicated in increasing resistance to carbapenems. Analysis of large KP genome collections, encompassing major healthcare-associated clones, revealed the recurrent emergence of a synonymous cytosine to thymine transition at position 25 (25c>t) in *ompK36.* We show that the 25c>t transition increases carbapenem resistance through depletion of OmpK36 from the outer membrane. The mutation attenuates KP in a murine pneumonia model, which accounts for its limited clonal expansion observed by phylogenetic analysis. However, in the context of carbapenem treatment, the 25c>t transition tips the balance towards treatment failure, thus accounting for its recurrent emergence. Mechanistically, the 25c>t transition mediates an intramolecular mRNA interaction between a uracil encoded by 25t and the first adenine within the Shine-Dalgarno sequence. This specific interaction leads to the formation of an RNA stem structure, which obscures the ribosomal binding site thus disrupting translation. While mutations reducing OmpK36 expression via transcriptional silencing are known, we uniquely demonstrate the repeated selection of a synonymous *ompK36* mutation mediating translational suppression in response to antibiotic pressure.

## Introduction

Classical outer membrane (OM) porins in Gram-negative bacteria enable non-specific bidirectional diffusion between the periplasm and extracellular environment (Achouak et al., 2001). This has been exploited in antibacterial chemotherapy as porins act as the key entry point for clinically important classes of antibiotics across the otherwise impermeable OM. However, porin modifications that restrict antibiotic entry have evolved in response to this selective pressure (Vergalli et al., 2020), contributing to the rising global burden of resistant bacterial infections, especially among species of *Enterobacteriaceae* (Bajaj et al., 2016; Dé et al., 2001; Wong et al., 2019; Fajardo-Lubián et al., 2019; Tran et al., 2010).

*Klebsiella pneumoniae* (KP) is one of the most clinically significant members of the *Enterobacteriaceae* family and a leading cause of healthcare-associated infections worldwide (Cassini et al., 2019; Vincent et al., 2020). The majority of resistant KP infections are caused by "high-risk" clonal lineages, including sequence types (ST) 258 and 512, which form a dominant clone associated with the KP carbapenemase (KPC) gene (David et al., 2019). Together with plasmid-encoded carbapenemases, modifications to the major OM porins OmpK35 and OmpK36 play a critical role in mediating KP resistance to carbapenems, a class of antibiotics that is vital for the treatment of severe infections. Resistance-associated modifications broadly fall into those that structurally alter the porin channel and those that abolish or reduce OmpK36 expression.

Structural alterations in OmpK36 are mediated by amino acid insertions into a region of the porin called loop 3 (L3). These insertions narrow the luminal diameter and restrict substrate diffusion, including antibiotics (Wong et al., 2019; Fajardo-Lubián et al., 2019).

42    L3 insertions are relatively prevalent among clinical KP isolates, having been found

43    among 12.3% (192/1557) of isolates from a diverse public genome collection (Fajardo-

44    Lubián et al., 2019). We previously showed that the most common L3 insertion, a di-

45    amino acid insertion (Glycine-Aspartate, GD), results in a 16-fold increase in minimum

46    inhibitory concentration (MIC) to meropenem (Wong et al., 2019).

47    In addition to structural modifications, carbapenem resistance is also achieved by absent

48    or reduced OmpK36 expression. Absent expression, which can be achieved by gene

49    truncation, results in high levels of resistance but comes at a significant *in vivo* fitness

50    cost (Wong et al., 2019; Fajardo-Lubián et al., 2019; Tsai et al., 2011). Reduced OmpK36

51    expression has been reported to occur by multiple mechanisms that all result from

52    transcriptional silencing, including *ompK36* promoter disruption by insertion sequence

53    (IS) elements (Clancy et al., 2013), loss-of-function mutations in *kvrA* (a transcriptional

54    repressor that controls capsule production) (Dulyayangkul et al., 2020) and mutations in

55    *hfq* (a regulatory RNA binding protein) (Chiang et al., 2011). However, the effects on

56    virulence resulting from reduced OmpK36 expression are poorly understood. Moreover,

57    the prevalence and clinical significance of these mechanisms remain unknown as the

58    mutations identified to date were either restricted to clinical isolates from a single centre

59    (promoter insertion) or evolved during *in vitro* selection or genetic deletion experiments

60    (*kvrA* and *hfq*).

61    Here we identify and describe a carbapenem resistance mechanism that has been

62    repeatedly employed by clinical KP isolates to post-transcriptionally alter OmpK36

63    abundance via synonymous mutations in the open reading frame (ORF). Our study spans

64    the identification of one such key mutation (25c>t) in *ompK36* through large-scale

65    bioinformatic approaches, the assessment of its effects on carbapenem susceptibility and

66    virulence using murine pneumonia models, and finally the determination of the precise

67    molecular mechanism linking synonymous SNPs with protein abundance. In particular,

68    we show that the 25c>t mutation results in the formation of a stem structure in the *ompK36*

69    mRNA that obscures the Shine Dalgarno sequence (SDS), reduces OmpK36 translation

70    and abundance, and increases carbapenem resistance as a consequence. This work

71    provides the first example of the functional use of these inhibitory mRNA structures in

72    regulating protein expression during bacterial adaptation, and characterises a novel,

73    clinically-important resistance mechanism in KP.

74 **Results**

75 ***Recurrent emergence of a synonymous 25c>t ompK36 mutation***

76 We curated and analysed a collection of 1450 public KP genomes belonging to the major

77 healthcare-associated clone composed of STs 258, 512 and other closely related

78 derivatives (https://microreact.org/project/1vWbaqARPRNc55n4yfdLyQ-ompk36; **Table**

79 **S1**). The collection comprises isolates gathered between 2003 and 2018, largely in the

80 Americas, Europe and the Middle East, where rampant spread of ST258/512 in

81 healthcare institutions has been reported (Adler et al., 2017; Giakkoupi et al., 2011; Giani

82 et al., 2013; Kitchel et al., 2009; Rojas et al., 2017). We unambiguously identified the

83 *ompK36* gene in 98.1% (1422/1450) of the genomes. Among these, the gene was intact

84 in 99.3% (1412/1422). Using the intact *ompK36* sequences, we inferred how each

85 position in this gene has evolved across the ST258/512 population. First, we constructed

86 a phylogeny of the collection using all vertically inherited single nucleotide polymorphisms

87 (SNPs) from a core genome alignment, with recombined regions excluded, to provide an

88 accurate representation of the ancestral relationships between isolates (Figure 1A). We

89 then mapped the variation in *ompK36* onto this phylogeny and predicted the ancestral

90 states of each position in the gene across the tree using a maximum parsimony approach.

91 While 83.4% of nucleotide positions are entirely conserved across *ompK36*, we found two

92 regions with an increased number of base changes (Figure 1B). As anticipated, the

93 largest number of changes occurred in the loop 3 (L3) region comprising amino acid

94 insertions (GD, TD, D and N) (24 occurrences) as well as their reversions (i.e. deletions)

95 (25 occurrences). However, further to this, we observed ten base changes at position 25,

96 all consisting of a synonymous c>t transition (CTG (leucine)->TTG (leucine)). Despite this

97 mutation maintaining the identical amino-acid translation in the Sec-dependent signal

98    sequence (Figure 2A&B), its high frequency of emergence suggests that it has undergone

99    positive selection. The majority of isolates with the 25c>t mutation are sporadically

100    distributed across the core genome phylogeny and occur as singletons or clusters of only

101    two isolates (11/18) (Figure 1A). The remaining seven isolates, collected between 2009

102    and 2013 from multiple healthcare institutions in the USA, form a monophyletic cluster,

103    indicative of a clonal expansion. We noted that these seven isolates encode an additional

104    synonymous 24c>t mutation in the preceding codon ((CT<u>C</u> (leucine)->CT<u>T</u> (leucine))

105    (Figure 2B).

106    We next searched for the 25c>t mutation in a large, geographically diverse collection of

107    16,086 KP genomes (https://pathogen.watch/genomes/all?genusId=570&speciesId=573;

108    Table S2) to establish its wider prevalence among sequenced isolates and presence in

109    other (i.e. non-ST258/512) clonal lineages. Among the 14,888 isolates encoding an intact

110    *ompK36* gene, we identified the 25c>t mutation in 2.5% (376/14,888), which includes

111    isolates from 39 STs and 25 countries. Over half (51.3%; 193/376) belong to ST258 while

112    many also belong to other globally-important multi-drug resistant clones (e.g. ST15,

113    19.9%; ST13, 4.5%; ST11, 2.7%). We observed the 24c>t mutation in 1.1% (161/14,888)

114    of genomes from this collection, and only ever in combination with the 25c>t mutation.

115    Moreover, we also noted that 93.2% (150/161) of *ompK36* sequences containing the

116    24&25c>t mutations had L3 insertions compared to only 1.9% (4/215) of those with 25c>t

117    only.

118    ***The 25c>t mutation increases meropenem resistance***

119    We modelled the effect of the 25c>t mutation (*ompK36*$_{WT(25c>t)}$) on meropenem resistance

120    by introducing the mutation into *ompK36*$_{WT}$ of our laboratory KP strain ICC8001 (Wong et

121  al., 2019) (see Table 1 for list of *ompK36* variants and strains used in this study). We

122  additionally deleted *ompK35*, as this porin gene is truncated in 99.8% of the ST258/512

123  genomes, and introduced the KPC-2 carbapenemase (on a pKpQIL-like plasmid) given

124  also the strong association of KPC genes with the lineage (Bowers et al., 2015). We found

125  that expression of *ompK36*$_{WT(25c>t)}$ results in a meropenem minimum inhibitory

126  concentration (MIC) of 64mg/L, 8-fold higher than the resistance breakpoint of 8mg/L

127  (EUCAST, 2021) (Figure 2C). This MIC is also four-fold higher than that seen in KP

128  expressing *ompK36*$_{WT}$ (16mg/L), albeit lower than the very high resistance observed

129  when *ompK36* was deleted (Δ*ompK36*, 512mg/L), indicating that the 25c>t is a

130  carbapenem resistance mutation.

131  We also investigated the level of resistance conferred by the combination of the 24c>t

132  and 25c>t mutations. While ICC8001 did not tolerate the genomic insertion of the double

133  24&25c>t mutations on a WT *ompK36* background, we found that they were tolerated

134  when introduced in combination with a L3 GD pore-constricting insertion

135  (*ompK36*$_{WT+GD(24&25c>t)}$). While we could not explain the inability to achieve

136  *ompK36*$_{WT(24&25c>t)}$ introduction, it nevertheless reflects the strong association between

137  the combined 24&25c>t mutations and L3 insertions observed in our genomic analysis.

138  Broth microdilution testing of the strain with *ompK36*$_{WT+GD(24&25c>t)}$, together with strains

139  encoding *ompK36*$_{WT+GD}$ and *ompK36*$_{WT+GD(25c>t)}$, revealed that the 25c>t mutation

140  increased the meropenem MIC of the L3 GD insertion strain from 64mg/L (WT+GD) to

141  256mg/L (WT+GD(25c>t)) and that the double 24&25c>t mutations partially reversed this

142  phenotype, with an MIC of 128mg/L (WT+GD(24&25c>t)) (Figure 2C).

143

144 ***ompK36*$_{WT(25c>t)}$ *attenuates virulence but tips the balance towards antibiotic therapy*

145 *failure*

146 The general absence of clonal expansion among isolates with the single 25c>t

147 substitution, despite the frequent emergence of this mutation, suggests that it may have

148 a fitness cost that impedes onward transmission. We tested this hypothesis *in vivo* by

149 infecting mice with 250 CFU of KP encoding either *ompK36*$_{WT}$ (KP36$_{WT}$) or

150 *ompK36*$_{WT(25c>t)}$ (KP36$_{WT(25c>t)}$) (Table 1). Inoculation with a strain encoding an *ompK36*

151 deletion (KPΔ36) and PBS were used as controls (Figure 3A). At 48 h post infection,

152 KP36$_{WT}$, but not KP36$_{WT(25c>t)}$, induced significant weight loss compared to uninfected

153 (PBS) mice or mice infected with KPΔ36, Figure 3B). Bacterial counts in the lungs showed

154 a trend to higher burdens in mice infected with KP36$_{WT}$ than with KP36$_{WT(25c>t)}$, which

155 reached significance in the blood (Figure 3C&D). KPΔ36 demonstrated defects in

156 bacterial survival and proliferation in the host, with significantly lower and/or absent

157 burdens in the lungs and blood (Figure 3C&D). Interferon gamma (IFNγ) is a key cytokine

158 in the defense against KP and measurement of its levels in serum provides a readout of

159 acute inflammatory responses (Moore et al. 2002); following infection with KP36$_{WT}$, IFNγ

160 responses were significantly higher compared to infection with KP36$_{WT(25c>t)}$ (Figure 3E).

161 Taken altogether, these findings show that the 25c>t transition attenuates KP *in vivo* with

162 reduced bacteraemia and the resulting induction of a diminished host pro-inflammatory

163 immune response.

164 We next evaluated if *ompK36*$_{WT(25c>t)}$ provides an advantage compared with *ompK36*$_{WT}$

165 in the context of meropenem therapy, which would explain the recurrent emergence of

166 this mutation despite its associated fitness cost. We infected mice with either KP36$_{WT}$ or

167 KP36$_{WT(25c>t)}$, both expressing the KPC-2 carbapenemase from a pKpQIL-like plasmid. At

168 24 h mice either received meropenem (100mg/kg dose) or vehicle control (water) by

169 intraperitoneal injection at six hourly intervals for 24 h (Figure 3F). The experiment was

170 stopped 3 h after the last injection. No significant differences in body weight were

171 observed following infection by either strain with or without meropenem therapy (Figure

172 3G), consistent with fluid resuscitation provided by meropenem or vehicle administration.

173 However, significant reductions in the bacterial burdens in the lungs and blood were seen

174 following meropenem treatment of KP36$_{WT}$+KPC-2 but not KP36$_{WT(25c>t)}$+KPC-2 infection

175 (Figure 3H&I). Furthermore, while the level of serum IFNγ was significantly decreased

176 when KP36$_{WT}$+KPC-2 infection was treated with meropenem (Figure 3J), no significant

177 differences were observed between antibiotic or mock treated KP36$_{WT(25c>t)}$+KPC-2

178 infected mice. These *in vivo* results show whilst the 25c>t mutation in *ompK36* attenuates

179 KP, it provides a selective advantage during carbapenem therapy.

180 ***The 25c>t mutation reduces OmpK36 abundance***

181 We next aimed to understand how the 25c>t mutation mediates an increase in

182 meropenem resistance and an associated decrease in virulence. Since the mutation

183 results in both carbapenem resistance and virulence phenotypes between those

184 observed in normal (*ompK36*$_{WT}$) and absent (Δ*ompK36*) expression, we hypothesized

185 that these phenotypic changes were due to reduced OmpK36 abundance in the OM.

186 Indeed, analysis of isolated OM fractions by SDS-PAGE and Coomassie staining

187 revealed that the strain encoding *ompK36*$_{WT(25c>t)}$ exhibited a substantially reduced

188 abundance of OmpK36 compared to that with *ompK36*$_{WT}$ (Figure 2D), validating this

189 hypothesis. In line with the meropenem MIC results, we also found that this pattern is

190    reversed in the strain encoding *ompK36*$_{WT+GD(24\&25c>t)}$, which exhibits OmpK36 levels

191    similar to the strain encoding *ompK36*$_{WT}$ (Figure 2D).

### Reduced OmpK36 abundance via the 25c>t mutation occurs independently of codon bias

194    We sought to describe the precise molecular mechanism linking the synonymous 25c>t

195    mutation to decreased OmpK36 abundance. We first explored whether reduced OmpK36

196    abundance is due to a decreased translation rate, resulting from a change in codon from

197    the commonly-used CTG to the rarely-used TTG at amino acid position 9 (Leu9). Overall,

198    64.9% of leucine residues in the ICC8001 genome are encoded by CTG and 5.9%

199    encoded by TTG (Figure 4A); inspection of all the ST258/512 genomes confirmed a

200    similar bias (CTG range: 57.0-65.1%; TTG range: 5.9-9.3%).

201    To investigate this, we generated a fluorescent ICC8001 reporter, in which the *ompK36*

202    ORF was replaced with the *ompK36* signal sequence fused to sfGFP (Figure 4B). This

203    reporter maintains the upstream promoter and regulatory regions at the monocistronic

204    *ompK36* locus. Using sfGFP fluorescence as a proxy for protein expression, we found

205    that the signal sequence containing the 25c>t mutation (TTG codon) significantly reduced

206    expression compared to that with the WT sequence (CTG codon) (Figure 4C). This finding

207    is consistent with the reduced OmpK36 abundance observed in the strain encoding

208    *ompK36*$_{WT(25c>t)}$ (Figure 2D). We then used the CTC leucine codon located at amino acid

209    position eight (Leu8) to test the impact of codon usage on expression. We generated

210    synonymous mutants where Leu8 was encoded by either of the alternative CTG

211    (common) or TTG (rare) codons. Both Leu8 CTG and TTG codons resulted in similar

212    sfGFP expression, which was significantly higher than with the CTC codon found in

213  *ompK36*<sub>WT</sub> (Figure 4C). This suggested that the underlying mechanism reducing OmpK36

214  expression via the 25c>t mutation is not related to codon usage limiting the efficiency of

215  translation elongation.

**Reduced OmpK36 abundance is mediated by an interaction between the ORF and**

**5'UTR**

218  Mutagenesis studies in *E. coli* have suggested that specific intramolecular RNA

219  interactions between nucleotides in the 5' end of an ORF and the upstream 5'UTR region

220  can result in secondary structures that occlude the SDS, blocking ribosomal access

221  (Kudla et al., 2009; Bhattacharyya et al., 2018). This disrupts the initiation of translation,

222  reducing protein expression, and in turn results in mRNA degradation as transcription and

223  translation are tightly coupled (Bhattacharyya et al., 2018). However, mutations reducing

224  translation efficiency have not been identified as a naturally occurring mechanism tuning

225  protein expression in adaptation to a host or environmental pressure. Nonetheless, we

226  hypothesized that the reduced abundance of OmpK36<sub>WT(25c>t)</sub> may be due to an inhibitory

227  mRNA secondary structure, mediated by a specific a/u base-pairing occurring between

228  an adenine within the 5' UTR of *ompK36* (Figure 4D) and the uracil encoded by 25t. We

229  started by confirming the lower abundance of *ompK36* mRNA transcripts in the 25c>t

230  mutant compared to WT by qRT-pCR (Figure 4E), a finding consistent with increased

231  mRNA degradation. We then individually mutated each adenine to a thymine (starting

232  from the end of the -10 box/transcription start site) in the 5'UTR of the sfGFP reporter

233  containing the 25c>t mutation in the signal sequence. We hypothesized that the disruption

234  of any base interaction between 25u and a position in the 5'UTR would be evidenced by

235  increased sfGFP expression. No significant changes in fluorescence were observed in

236  adenine substitutions up to and including the -16 position (Figure 4F). However,

237  substitution of -14a, which marks the start of the SDS, abolished the effect of 25c>t on

238  sfGFP signal suppression, with significantly increased fluorescence in the strain encoding

239  the 14a>t mutation (p<0.001). In order to exclude the possibility that -14a>t had a non-

240  specific effect on the functionality of the SDS due to enhanced ribosomal binding, we

241  introduced -14a>t in the WT reporter (without 25c>t). Similar signal levels were observed

242  in both reporters (-14a/25c and -14t/25c), suggesting that -14a>t alone does not affect

243  protein expression (Figure 4G).

244  We next investigated the effect of the -14a>t mutation on OmpK36 abundance in the

245  context of *ompK36*$_{WT}$ and *ompK36*$_{WT(25c>t)}$. As expected, no effect on abundance was

246  observed when the mutation was introduced into *ompK36*$_{WT}$ (Figure 4H). In contrast,

247  introduction of the -14a>t mutation in the 5'UTR of *ompK36*$_{WT(25c>t)}$ increased OmpK36

248  abundance (Figure 4H). These findings therefore suggest that the 25c>t mutation may

249  result in an inhibitory mRNA secondary structure via a specific interaction with position -

250  14 in the 5'UTR.

251  ***The 25c>t mutation induces an mRNA stem loop structure involving the Shine-***

252  ***Dalgarno sequence***

253  To test the hypothesis that the 25c>t mutation results in an mRNA interaction between -

254  14a and 25u that obstructs the SDS and prevents ribosome recruitment, we probed the

255  structures of the *ompK36*$_{WT}$ and *ompK36*$_{WT(25c>t)}$ mRNAs using dimethyl sulfate (DMS)

256  mutational profiling with sequencing (DMS-MaPseq) (Zubradt et al., 2017). This technique

257  uses DMS modifications of adenine and cytosine bases in the RNA, detected as

258  mismatches during reverse transcription, to infer the accessibility of individual bases and

259  subsequently build a model of the RNA structure. We found that adenine and cytosines

260    within the SDS are more accessible to DMS in *ompK36*WT mRNA than *ompK36*WT(25c>t)

261    mRNA both *in vitro* and *in vivo* (Figures 5A, 5B, Figure S1). Introducing the 24c>u

262    mutation in addition to 25c>u reversed the DMS accessibility of the SDS to that

263    resembling *ompK36*WT (Figure 5C). As a negative control, we also tested a sample with

264    no DMS treatment, which indeed showed minimal background signal (Figure 5D).

265

266    Correlation of the DMS signals between different pairs of *ompK36* variants (from positions

267    -16 to +28) further demonstrated higher similarity between *ompK36*WT and

268    *ompK36*WT(24&25c>t) than between *ompK36*WT and *ompK36*WT(25c>t) (Figure 5E-G).

269    This implies that the RNA structure of the double mutant more closely resembles the WT.

270    Indeed, DMS-driven structure models showed visually that the SDS is largely accessible

271    for both the WT and the double mutant (although uncertainty exists in the model post

272    position 13 of the double mutant) (Figures 5H-J, SI). In contrast, the SDS in

273    *ompK36*WT(25c>t) is sequestered into a stem structure, which incorporates the paired

274    positions of -14 and 25. These results provide direct evidence that RNA structure

275    occluding the SDS underlies the reduced expression of OmpK36 in strains encoding the

276    25c>t mutation. Altogether, these findings provide the precise molecular mechanism

277    linking the occurrence of synonymous SNPs to altered OmpK36 abundance and

278    meropenem resistance levels.

**Discussion**

OmpK36 is a key porin in KP, reflected by its typically high abundance in the outer membrane. However, its role in facilitating antibiotic entry has exerted an evolutionary pressure favouring mutations that restrict this process (Vergalli et al., 2020). Using large clinical genome collections, we identified a single, recurrently-emerging synonymous base substitution at the 25th nucleotide position of *ompK36* that increases carbapenem resistance by reducing OmpK36 expression. We observed that this 25c>t mutation usually occurs in the absence of L3 insertions, unless a 24c>t mutation which reverses the phenotype is also present, demonstrating that KP typically uses either OmpK36 pore constriction (via L3 insertions) or reduced OmpK36 abundance as a means for increasing resistance. Mechanistically, we show the significant impact a single synonymous substitution can have on protein expression, through the induction of a dramatic mRNA conformational change. To the best of our knowledge, this is the first time an adaptive mutation that restricts translation initiation has been shown to occur naturally.

In unravelling the molecular mechanism, our *in vitro* mutagenesis experiment showed that reduced OmpK36 expression via the 25c>t mutation is the result of a specific interaction between 25u in the mRNA and the first adenine base at the upstream SDS (-14a). The interaction was confirmed by solving mRNA structures with DMS-MaPseq. This technique revealed large conformational differences in the structures of the *ompK36*<sub>WT</sub> and *ompK36*<sub>WT(25c>t)</sub> transcripts, including the presence of a stem loop structure sequestering the SDS only in the *ompK36*<sub>WT(25c>t)</sub>. We propose that this stem loop structure, triggered by the interaction between 25u and -14a, impedes ribosomal binding and thereby reduces translation efficiency. Further evidence for this proposed mechanism also came from the mRNA transcript model of *ompK36*<sub>WT(24&25c>t)</sub> (these double mutations also having been

303  observed among clinical isolates), which again had a different conformation but showed

304  no stem loop structure obscuring the SDS. This could explain the reversal of the

305  phenotypes observed in this mutant compared with that encoding only 25c>t. Indeed,

306  previous studies have demonstrated that experimentally-induced mRNA secondary

307  structures near the SDS decrease protein levels using a synthetic library of synonymous

308  GFP variants (Kudla et al., 2009) and, more recently, using two endogenous genes in *E.*

309  *coli* (Bhattacharyya et al., 2018). Crucially, however, it has been proposed that the base

310  composition at the start of genes has evolved to minimise the formation of these

311  structures, as evidenced by a genome-wide analysis in *E. coli* (Bhattacharyya et al.,

312  2018). This appears to be the case in the *ompK36*$_{WT}$ transcript, in which the SDS lies in

313  a largely open conformation. However, the mechanism behind the increased resistance

314  of the 25c>t mutant (and reversal of this phenotype in the 24&25c>t mutant) extends our

315  understanding of this system by demonstrating that mutations which induce alternative

316  secondary structures can also be selected during adaptation. Importantly it also provides

317  a demonstration of the functional use of these inhibitory mRNA structures in regulation

318  among naturally occurring and clinically relevant populations.

319  In keeping with the key role of OmpK36 in maintaining KP physiology, we demonstrated

320  that the 25c>t mutation decreased bacterial replication in a murine pneumonia model.

321  This correlated with reduced levels of serum IFNγ which plays an important role in KP

322  lung infection in mice (Yoshida et al. 2001; Moore et al., 2002). Our phylogenetic analyses

323  suggested that this level of attenuation may be enough to impact on transmission, with

324  most isolates possessing this mutation forming singletons or pairs in the ST258/512

325  phylogeny (i.e. not being part of larger clonal expansions). Moreover, despite its frequent

326  emergence, the total prevalence of the 25c>t mutation among the ST258/512 genome

327  collection remained at 1.2%. This is similar to the prevalence of loss-of-function mutations

328  in *ompK36* (0.7%) but is in sharp contrast to L3 insertions, which have spread widely via

329  large clonal expansions to reach a prevalence of 47.0%. Nevertheless, despite the limited

330  clonal expansion of 25c>t, our identification of this mutation in clinical isolates

331  demonstrates that it does not preclude infection in patients.

332  Using our translational model of pneumonia, we could further show that the increased

333  resistance conferred by the 25c>t mutation was enough to result in a clinical impact,

334  thereby explaining its recurrent emergence (despite the fitness cost). Mice infected with

335  KP expressing *ompK36*$_{WT}$+KPC-2 could be successfully treated with meropenem, while

336  those infected with KP possessing *ompK36*$_{WT(25c>t)}$+KPC-2 could not. We therefore

337  propose that the repeated emergence of 25c>t is driven by antibiotics, possibly due to

338  prolonged exposure and/or subtherapeutic dosing; both are commonly encountered

339  among critically ill patients, in whom antibiotic pharmacokinetics are difficult to predict at

340  an individual patient level (Roberts et al., 2014). Indeed, porin modifications occurring

341  within the time course of a single infection have been reported previously (Elliott et al.,

342  2006; Yoshino et al., 2021), demonstrating potential for their emergence and selection

343  given strong antibiotic pressure. Increased host susceptibility due to co-morbidity and

344  impaired immune responses in the population most at risk of KP disease could also render

345  the associated fitness cost of 25c>t less significant.

346  While the frequency of 25c>t has remained low, we propose that its ongoing *de novo*

347  emergence, together with the spectrum of other known OmpK36 modifications, impose a

348  significant impact on patient treatment. Moreover, porin mutations that reduce

349  carbapenem entry are not restricted to KP and are found in other WHO critical priority

350  organisms such as *Pseudomonas aeruginosa* and *Escherichia coli* (Bajaj et al., 2016;

351    Lister et al., 2009). This highlights the need for the development of novel effective

352    antibiotic therapies that circumvent reliance on diffusion through porins. While this has

353    been achieved via the newly licensed cephalosporin, cefiderocol, which instead enters

354    via siderophore uptake systems (Kohira et al., 2016), additional drugs are still needed.

355    In summary, our combined genomic, experimental and translational approaches have

356    uncovered a novel mechanism underpinning carbapenem resistance, mediated by

357    synonymous mutations that alter *ompK36* mRNA secondary structure. The associated

358    dynamics of emergence and expansion of these mutations are at the heart of an

359    evolutionary conflict balancing resistance and virulence requirements in KP. We propose

360    a central role for combining genomic surveillance with *in vitro* and translational evaluation

361    to further our understanding of resistance mutations, and to design and target our clinical

362    interventions accordingly.

**Author contributions**

JLCW and SD conceived the study. SD performed bioinformatics and genomic analyses. JLCW performed the molecular biology and biochemistry experiments. WWL performed the outer membrane preparations. JLCW, JSG and WWL performed the animal experiments under the supervision of GF. JSG performed cytokine measurements. FM, TG and GMR performed the meropenem resistance assays. JZW performed the DMS-MaPseq under the supervision of SR. Data analysis was carried out by JLCW, SD and JSG. JLCW, SD and GF wrote the manuscript. All authors reviewed and edited the manuscript (JLCW, SD, JSG, JZW, WWL, FM, TG, GMR, SJB, AC, DMA, SR and GF).
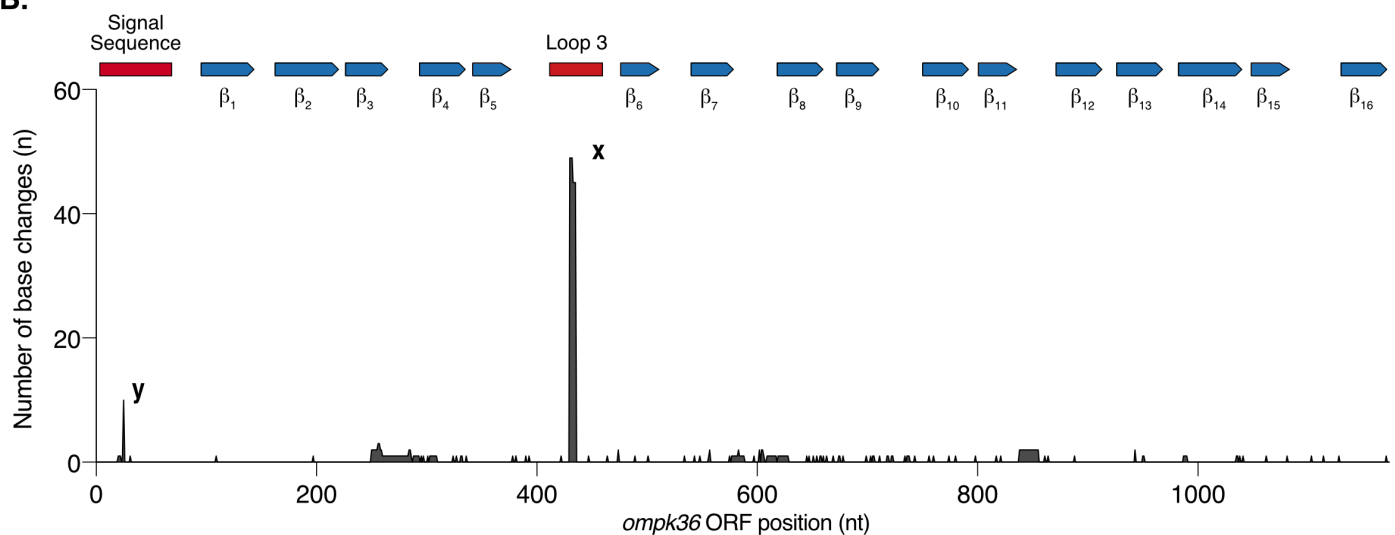
**Declaration of Interests**

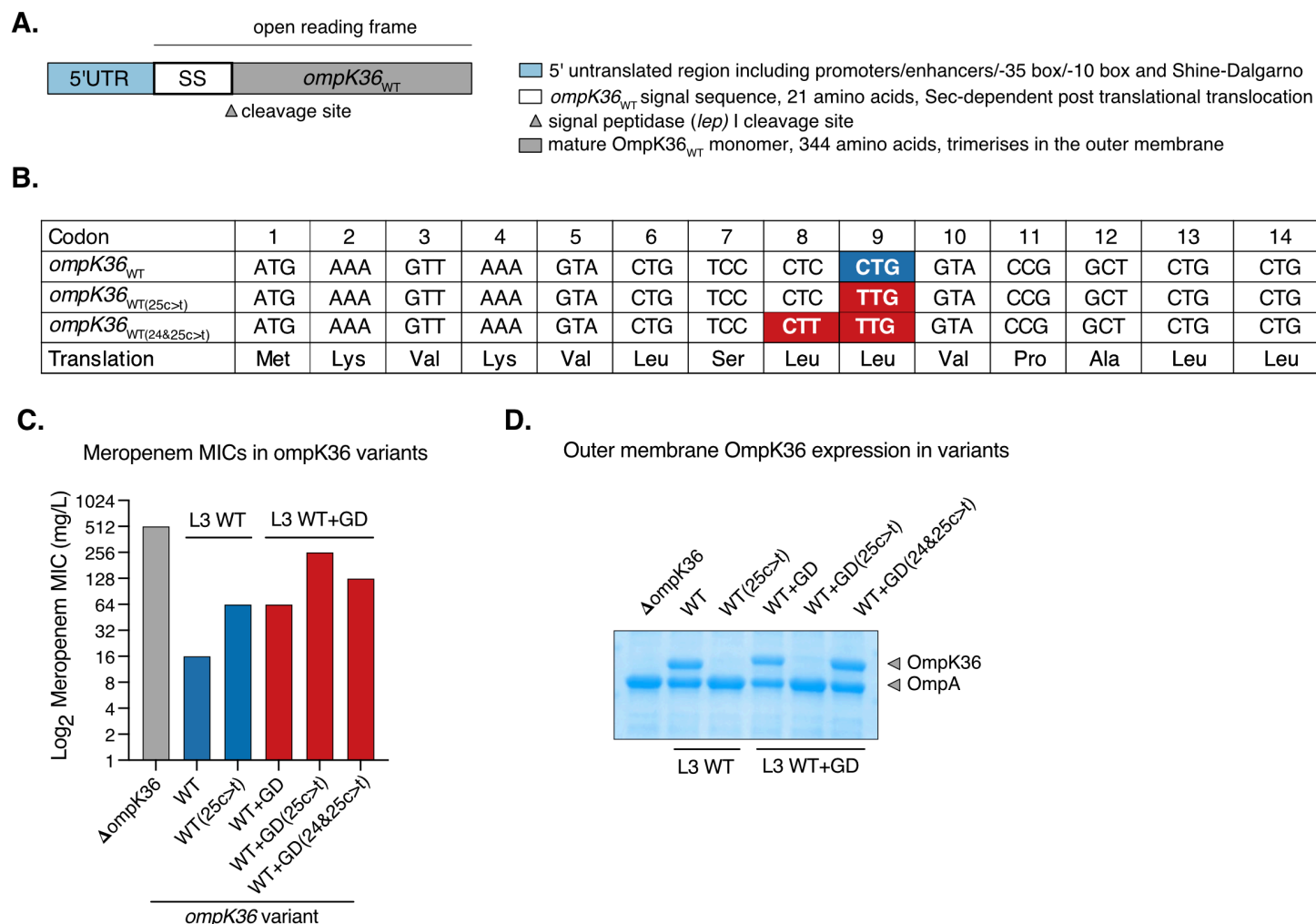Authors declare that they have no competing interests.

**Figure 1.**

**A.**



**B.**
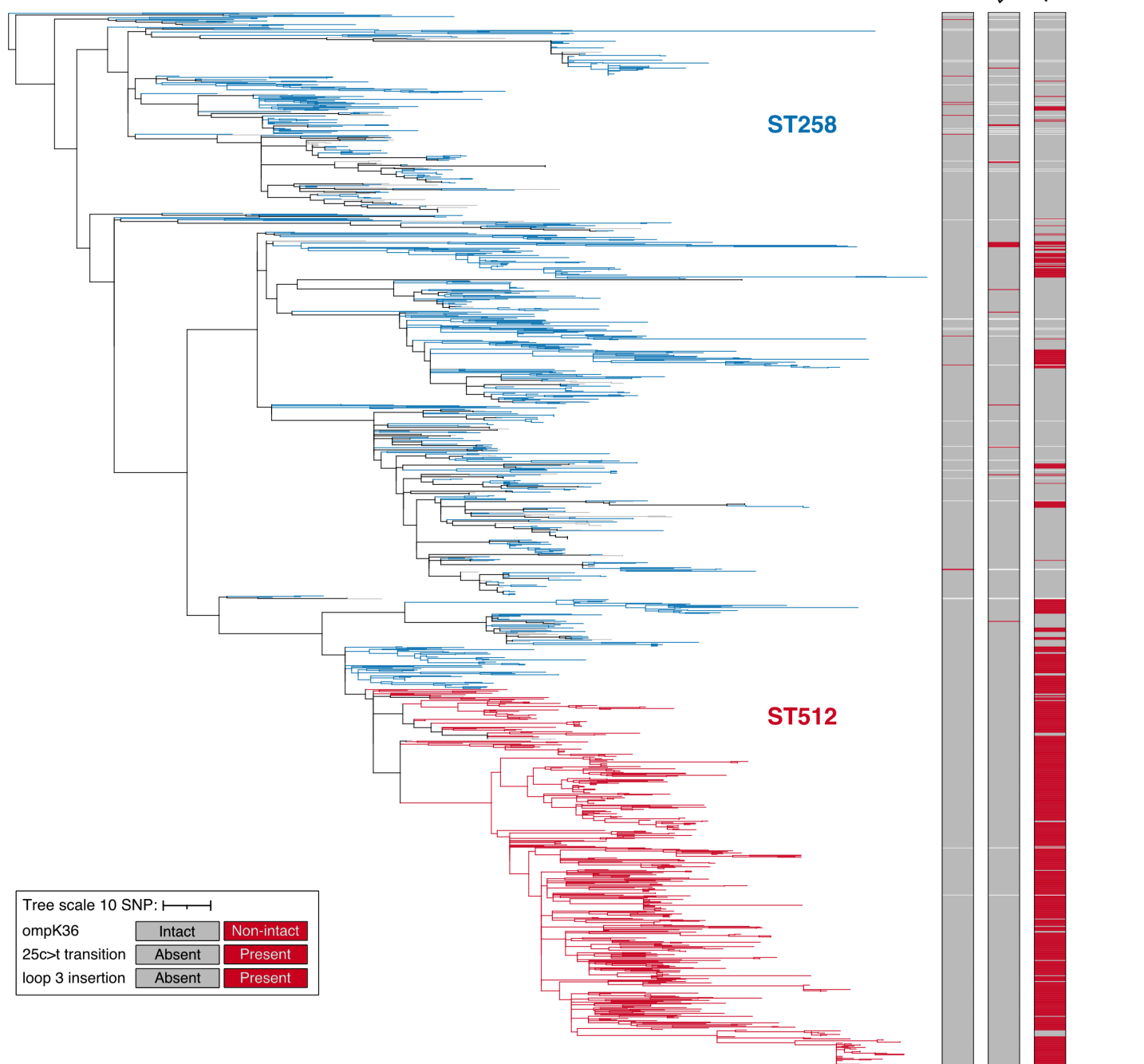
386 **Figure. 1. Frequency and phylogenetic distribution of *ompK36* variants in a curated**

387 **collection of ST258/512 genomes.**

388 **A.** Phylogenetic tree of 1450 KP ST258/512 isolates constructed using vertically-inherited

389 single nucleotide polymorphisms (SNPs). Branches are coloured blue if all descendent

390 taxa belong to ST258, red if they belong to ST512, grey if they belong to other closely

391 related derivatives of these STs, or black if they belong to one or more of these different

392 categories. Data columns (L-R) show *ompK36* (intact/non-intact)*, ompK36* 25c>t

393 transition (present/absent) and *ompK36* loop 3 (L3) insertion (present/absent) in each

394 genome. Isolates are marked white if *ompK36* could not be unambiguously identified in

395 the genome (columns 1-3) or if *ompK36* was non-intact (columns 2/3). The scale

396 represents the number of SNPs per variable site. A similar visualisation is available at:

397 https://microreact.org/project/1vWbaqARPRNc55n4yfdLyQ-ompk36#wksn-figure-1a-

398 wong-et-al-2022.

399 **B.** The number of changes (including SNPs, insertions and deletions) at each position in

400 *ompK36* detected across the ST258/512 tree. The protein structure motifs (signal

401 sequence, beta strands 1-16 and L3) are plotted on top of the sequence as a reference.

402 The labelled peaks represent insertions/reversions within the L3 (x) and the 25c>t

403 mutation found within the signal sequence (y).

404

**Figure 2.**

**A.**



open reading frame

| 5'UTR | SS | ompK36_{WT} |

△ cleavage site

☐ 5' untranslated region including promoters/enhancers/-35 box/-10 box and Shine-Dalgarno
☐ ompK36_{WT} signal sequence, 21 amino acids, Sec-dependent post translational translocation
△ signal peptidase (lep) I cleavage site
☐ mature OmpK36_{WT} monomer, 344 amino acids, trimerises in the outer membrane

**B.**

| Codon | 1 | 2 | 3 | 4 | 5 | 6 | 7 | 8 | 9 | 10 | 11 | 12 | 13 | 14 |
|---|---|---|---|---|---|---|---|---|---|---|---|---|---|---|
| ompK36_{WT} | ATG | AAA | GTT | AAA | GTA | CTG | TCC | CTC | CTG | GTA | CCG | GCT | CTG | CTG |
| ompK36_{WT(25c>t)} | ATG | AAA | GTT | AAA | GTA | CTG | TCC | CTC | TTG | GTA | CCG | GCT | CTG | CTG |
| ompK36_{WT(24&25c>t)} | ATG | AAA | GTT | AAA | GTA | CTG | TCC | CTT | TTG | GTA | CCG | GCT | CTG | CTG |
| Translation | Met | Lys | Val | Lys | Val | Leu | Ser | Leu | Leu | Val | Pro | Ala | Leu | Leu |

**C.**

Meropenem MICs in ompK36 variants



**D.**

Outer membrane OmpK36 expression in variants



◁ OmpK36
◁ OmpA

L3 WT    L3 WT+GD

**Figure. 2. ompK36_{WT(25c>t)} leads to increased meropenem MIC and reduced OmpK36 abundance.**

**A.** Schematic of the ompK36 locus.

**B.** The synonymous 25c>t mutation occurs at codon position 9 (Leu9) resulting in a change of codon from CTG (ompK36_{WT}) to TTG (ompK36_{WT(25c>t)}). The 24c>t mutation occurs in position 8 (Leu8) resulting in a synonymous CTC to CTT codon switch.

**C.** The 25c>t transition increases the meropenem resistance achieved on both a WT and WT+GD ompK36 background. The additional 24c>t (WT+GD(24&25c>t)) mutation partially reverses the resistance achieved in the 25c>t transition.

21

415    All strains harbour a pKpQIL-like plasmid expressing KPC-2 and have *ompK35* deleted.

416    Resistance values represent broth MICs (median of 3 repeats).

417    **D.** Representative Coomassie gel image of outer membrane (OM) preparations

418    demonstrating the reduced OmpK36 expression conferred by 25c>t in both WT and

419    WT+GD backgrounds. The additional 24c>t in WT+GD(24&25c>t) reverses the OM

420    depletion of OmpK36 in WT+GD(25c>t).

421

**Figure 3.**
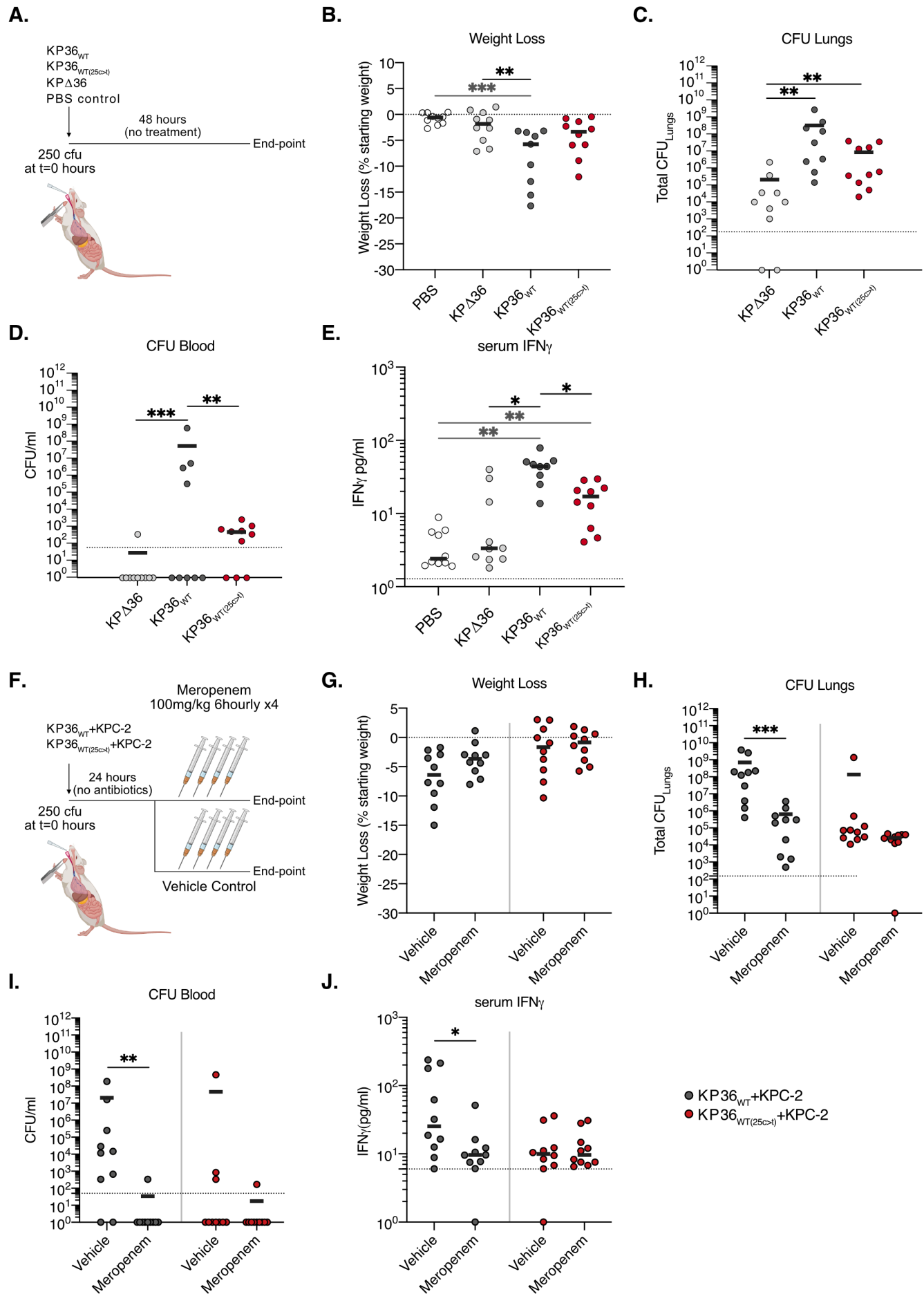
**423**  **Figure. 3. The 25c>t mutation has a fitness cost *in vivo* but is advantageous in the**

**424**  **context of meropenem therapy.**

**425**  **A-E.** Mice were infected by intubation and administration of 250 CFU of KP36$_{WT}$,

**426**  KP36$_{WT(25c>t)}$ or KPΔ36 strains; mock infection with PBS was used as a control. A

**427**  schematic of the infection protocol is outlined in panel a.

**428**  **B.** Animals infected with KP36$_{WT}$ show greater weight loss after 48 h compared to mock-

**429**  infected animals and those infected with KPΔ36. Weight loss in animals infected with

**430**  KP36$_{WT(25c>t)}$ is not significantly different to that of the PBS or KPΔ36 groups.

**431**  **C** and **D**. Enumeration of CFU in lungs and blood, collected at 48 h post infection, reveals

**432**  that infection with KPΔ36 does not result in high lung bacterial burdens and bacteraemia.

**433**  Infection with KP36$_{WT}$ results in high pulmonary bacterial burdens (**C**) and bacteraemia

**434**  (**D**), while infection with KP36$_{WT(25c>t)}$ results in a trend towards lower pulmonary bacterial

**435**  counts and reduced levels of bacteria in the blood. Dotted line represents the limit of

**436**  detection of the assay.

**437**  **E.** Infection with KP36$_{WT}$ or KP36$_{WT(25c>t)}$ leads to increased serum IFNγ compared to

**438**  mock-infected (PBS) animals. KP36$_{WT(25c>t)}$ infection results in significantly reduced

**439**  serum IFNγ levels compared to KP36$_{WT}$ infection.

**440**  **F-J.** Mice were administered with KP36$_{WT}$+KPC-2 or KP36$_{WT(25c>t)}$+KPC-2 strains and

**441**  subjected to a meropenem dosing regimen to assess the success of antibiotic therapy in

**442**  KP-induced severe pneumonia. A schematic of the infection protocol is outlined in panel

**443**  **F**.

**444**  **G.** No changes were observed in weight loss between meropenem and vehicle control

**445**  therapy when experimental pneumonia induced by either KP36$_{WT}$+KPC-2 or

**446**  KP36$_{WT(25c>t)}$+KPC-2.

447    **H** and **I.** CFU enumeration in lungs (**H**) and blood (**I**) shows significant reduction in

448    meropenem-treated animals infected with KP36$_{WT}$+KPC-2 compared to vehicle treated

449    animals; levels of bacteraemia were undetectable in all but one meropenem treated

450    animal. Meropenem treatment has no impact on lung or blood CFUs in animals infected

451    with KP36$_{WT(25c>t)}$+KPC-2.

452    **J.** Serum levels of IFNγ are significantly reduced after meropenem treatment in animals

453    infected with KP36$_{WT}$+KPC-2; cytokine levels are not affected by meropenem treatment

454    in animals infected with KP36$_{WT(25c>t)}$+KPC-2.

455    Graphs show median values of 2 biological repeats (4-5 mice per group). Statistical

456    significance was determined by one-way ANOVA with Tukeys´s multiple comparison

457    post-test. *, $P < 0.05$; **, $P < 0.01$; ***$P < 0.001$; ****, $P<0.0001$ in **B-E**. The statistical

458    significance of the comparisons between vehicle and meropenem-treated animals was

459    determined via a non-parametric Mann-Whitney test. *, $P < 0.05$; **, $P < 0.01$; ***$P < 0.001$

460    in **G-J**.

**Figure 4.**



461
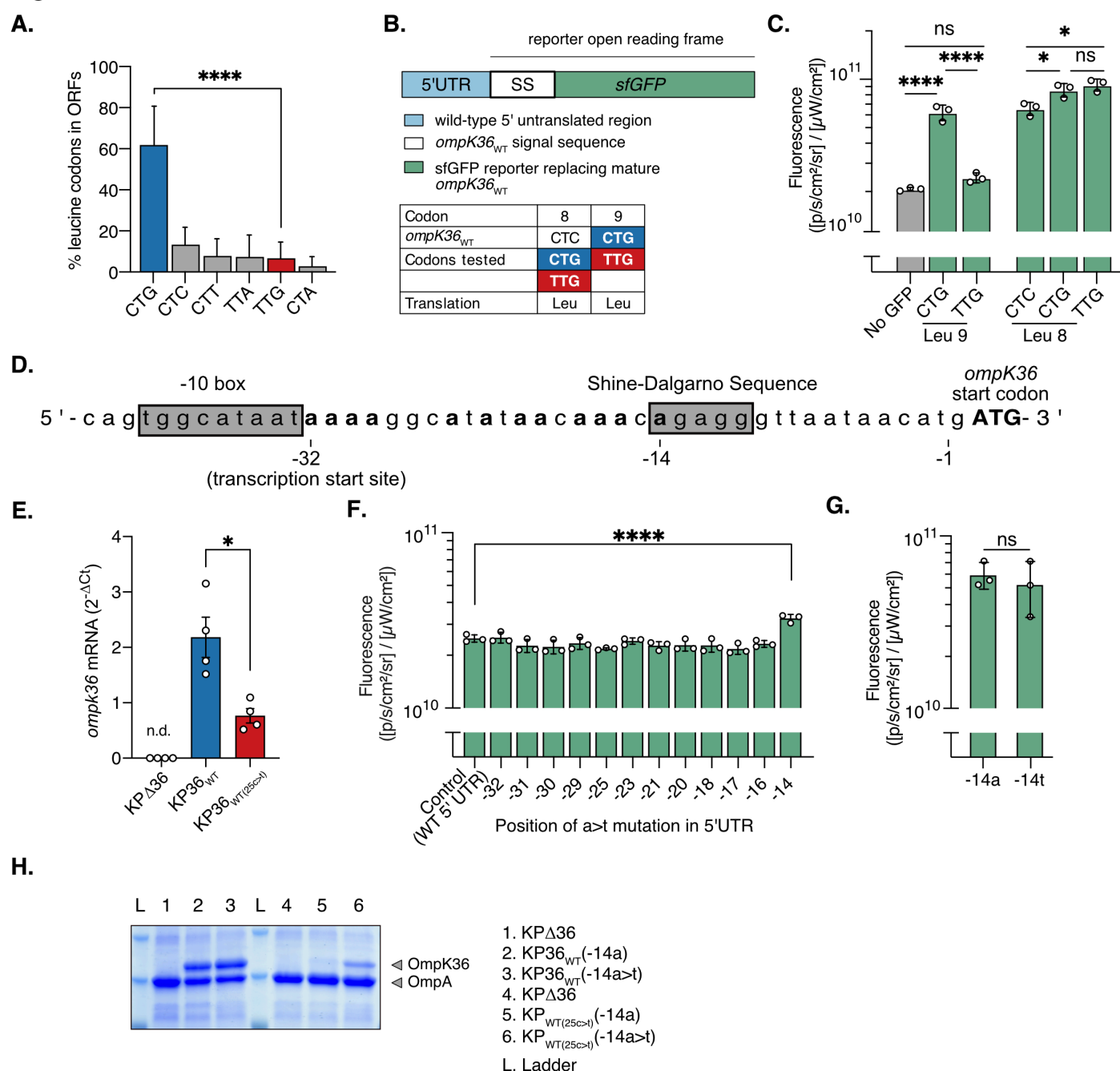
**Figure 4. The 25c>t mutation results in a specific intramolecular interaction between -14a and 25u in the mRNA transcript.**

**A.** Proportion of leucine residues encoded by each of the six codons across individual open reading frames (ORFs) in the ICC8001 KP genome. A significant difference was

26

466 observed in the use of CTG relative to TTG; significance was determined by paired T-test

467 ****, p<0.0001.

468 **B.** Schematic of the sfGFP reporter. The sequence encoding the mature OmpK36 protein

469 was replaced with sfGFP, generating a chimeric fusion between the *ompK36*$_{WT}$ signal

470 sequence (Leu9 CTG) and sfGFP. The inset table describes the mutations that were

471 introduced.

472 **C.** Mutation of Leu9 CTG (*ompK36*$_{WT}$) to TTG (*ompK36*$_{WT(25c>t)}$) decreases expression of

473 the sfGFP reporter. Mutations in Leu8 (CTC codon in *ompK36*$_{WT}$) to CTG or TTG codons

474 lead to similarly increased levels of reporter expression. Fluorescence was determined

475 using IVIS SpectrumCT. Graphs show means of 3 biological repeats ± the standard

476 deviation (SD). Statistical significance was determined by one-way ANOVA with Tukey´s

477 multiple comparison test. ns, not significant; *, P<0.05; ****, P<0.0001.

478 **D.** Sequence of the *ompK36* 5'UTR. Adenine bases in the 5'UTR (in bold) were

479 individually mutated to thymine.

480 **E.** RT-qPCR analysis of *ompK36* shows decreased transcript levels in the strain encoding

481 *ompK36*$_{WT(25c>t)}$ compared to *ompK36*$_{WT}$. Bar charts show the mean ± the standard error

482 of the mean (SEM) of 4 biological repeats. nd, not detected. ***P < 0.005 by paired

483 Student's *t* test.

484 **F.** Expression of the sfGFP reporter encoding the *ompK36*$_{WT(25c>t)}$ signal sequence is

485 specifically increased upon mutation of the adenine in position -14 to thymine (-14a>t).

486 The -14a marks the start of the Shine-Dalgarno sequence (SDS). Fluorescence was

487 determined using IVIS SpectrumCT. Graphs show the means ± SD of 3 biological repeats.

488 Statistical analysis was performed by one-way ANOVA with Dunnett´s multiple

489 comparison post-test. ****, P<0.0001.

490    **G.** Mutation of the adenine in position -14 to thymine (-14a>t) in the reporter construct

491    encoding the *ompK36*<sub>WT</sub> signal sequence (Figure 4B) does not impact sfGFP expression.

492    Bar charts show the mean ± the standard deviation (SD) of 3 biological repeats. *ns*, not

493    significant by paired Student's *t* test.

494    **H.** Representative Coomassie gel image of outer membrane preparations from isogenic

495    KP strains with the indicated *ompK36* mutations in positions -14 (5'UTR) and 25 (ORF

496    signal sequence). Mutation of the adenine in position -14 to thymine (-14a>t) restores

497    expression of OmpK36 in the presence of the 25c>t mutation*.*

**Figure 5.**
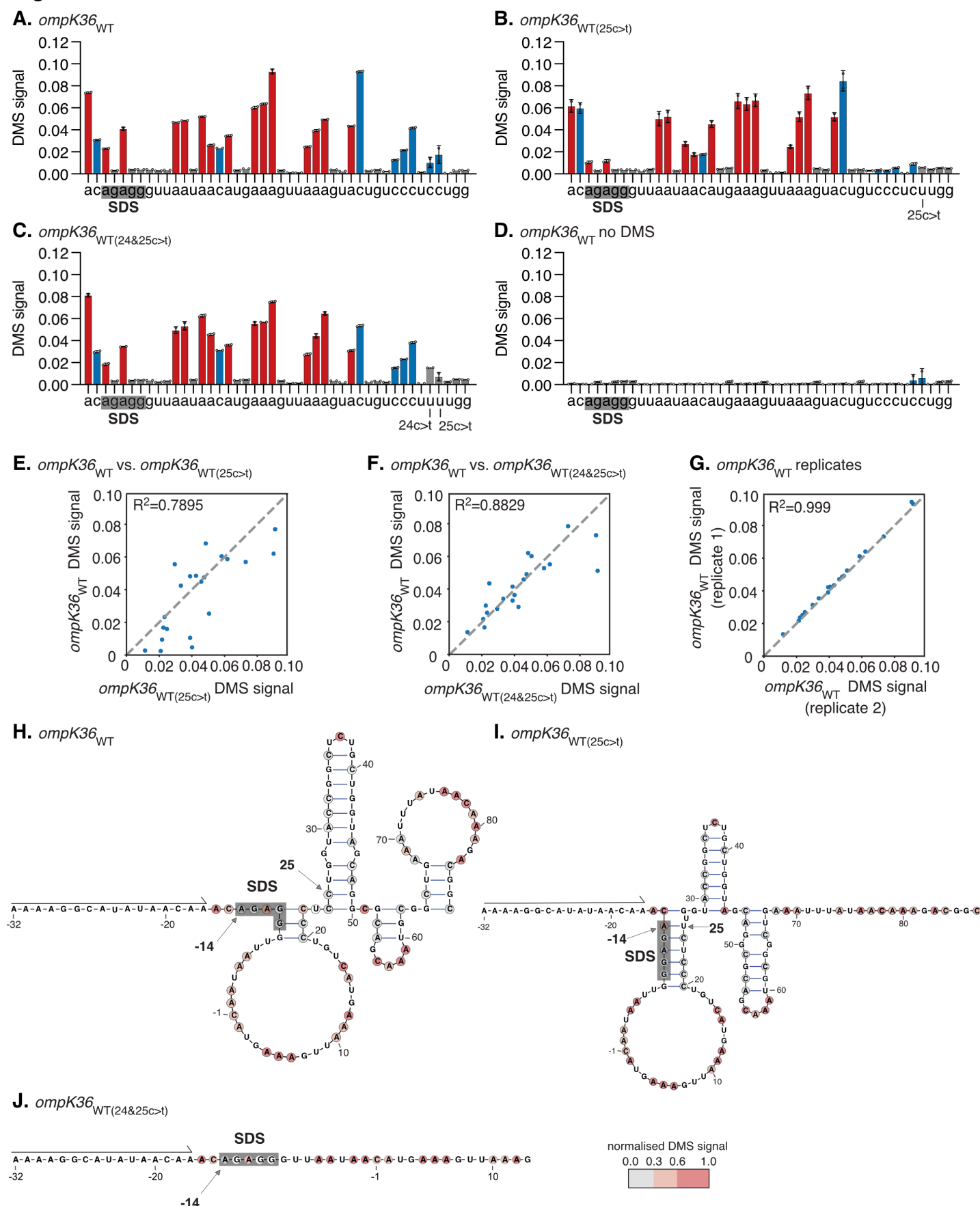
499 **Figure 5. Position 25 in the *ompK36*<sub>WT(25c>t)</sub> RNA induces a stem involving the Shine-**

500 **Dalgarno sequence (SDS).**

501 **A-D** Dimethyl sulfate (DMS) signal per nucleotide from full length *in vitro*-transcribed and

502 refolded *ompK36*, where higher values correspond to increased base accessibility. DMS

503 signal and error bars for nt -16a through 28g are shown for *ompK36*<sub>WT</sub>

504 (**A**), *ompK36*<sub>WT(25c>t)</sub> (**B**), *ompk36*<sub>WT(24&25c>t)</sub> (**C**) and DMS-untreated *ompK36*<sub>WT</sub> (**D**).

505 **E-G**. Comparison of DMS reactivities from nucleotides -16a through 28g between

506 *ompK36*<sub>WT</sub> and *ompK36*<sub>WT(25c>t)</sub> (**E**), between *ompK36*<sub>WT</sub> and *ompk36*<sub>WT(24&25c>t)</sub> (**F**), and

507 between *ompK36*<sub>WT</sub> replicates (**G**). Pearson correlations ($R^2$) are shown.

508 **H-J**. DMS-constrained structure models of the 5' end of *ompK36*<sub>WT</sub> (**H**), *ompK36*<sub>WT(25c>t)</sub>

509 (**I**) and *ompK36*<sub>WT(24&25c>t)</sub> (**J**). Nucleotides are colored by normalized DMS signal. The

510 PCR primer binding sites where DMS information is unavailable are marked from

511 positions -32 to -17. The SDS in RNA structures are highlighted in grey. Arrows indicate

512 the -14 and +25 positions.

513

514 **Supplementary Figure Legends**

515 **Figure S1. Position 25 in the *ompK36*<sub>WT(25c>t)</sub> RNA forms a stem with the Shine-**

516 **Dalgarno sequence (SDS) *in vivo*.**

517 **A.** Dimethyl sulfate (DMS)-constrained predicted structures of *in vivo ompK36*<sub>WT</sub> (top) and

518 *ompK36*<sub>WT(25c>t)</sub> (bottom) RNA molecules. Nucleotides are colored by normalized DMS-

519 MaPseq mutation rate (DMS signal), where higher values correspond to increased base

520 accessibility. The PCR primer binding site where DMS information is unavailable is

521 highlighted. *In vivo* RNA structures correspond with *in vitro* transcribed RNA structures

522    (Figure 5A&B) with SDS sequestration in the *ompK36*<sub>WT(25c>t)</sub> but not *ompK36*<sub>WT</sub> RNA

523    molecule.

524    **B.** Correlation of DMS signals for each nucleotide between two biological replicates for

525    *in vivo ompK36*<sub>WT</sub> (top) and *ompK36*<sub>WT(25c>t)</sub> (bottom).

526    **C.** DMS signal per nucleotide of *in vivo ompK36*<sub>WT</sub> (top) and *ompK36*<sub>WT(25c>t)</sub> (middle) and

527    DMS-untreated *ompK36*<sub>WT</sub> (bottom) RNA molecules. The SDS are highlighted in grey

528    boxes.

**Tables**

**Table 1.** *ompK36* **variants and KP strains used in this study.**

| *ompK36* variants | Nucleotide at | Nucleotide at | Loop 3 (L3) insertion |
|---|---|---|---|
| *ompK36*$_{WT}$ | c | c | Absent |
| *ompK36*$_{WT(25c>t)}$ | c | t | Absent |
| *ompK36*$_{WT+GD}$ | c | c | Glycine-Aspartate (GD) |
| *ompK36*$_{WT+GD(25c>t)}$ | c | t | Glycine-Aspartate (GD) |
| *ompK36*$_{WT+GD(24\&25c>t)}$ | t | t | Glycine-Aspartate (GD) |
| **Strains** | ***ompK35*** | ***ompK36*** | **Carbapenemase** |
| KPΔ36 | Δ | Δ | +/- KPC-2* |
| KP36$_{WT}$ (+/- KPC-2) | Δ | *ompK36*$_{WT}$ | +/- KPC-2* |
| KP36$_{WT(25c>t)}$ (+/- KPC-2) | Δ | *ompK36*$_{WT(25c>t)}$ | +/- KPC-2* |

*KPC-2 on pKpQIL-like plasmid

**Supplementary Table Legends**

**Table S1.** Metadata and genotyping data for a curated collection of 1450 KP ST258/512 genomes.

**Table S2**. Metadata and genotyping data for 16,086 KP genomes available in Pathogenwatch.

32

538 **Methods**

539 Genome collections

540 We used two genome collections to characterise the diversity and phylogenetic

541 distribution of *ompK36* (and *ompK35*) variants. The first comprises 1450 public KP

542 genomes belonging to STs 258, 512 and other nested STs, together with curated

543 metadata obtained from associated publications (**Table S1**). We obtained raw sequence

544 reads if available (1340 isolates), and short-read assemblies from the remainder (110

545 isolates). Assemblies were generated for all isolates with available raw sequence data

546 using SPAdes v3.9.0 (Bankevich et al., 2012), and annotated with Prokka v1.14.5

547 (Seemann, 2014). Kleborate v1.0.0 (Lam et al., 2021) was used for confirming the ST of

548 each genome and determining the resistance gene content.

549 The second collection comprises a public genome collection of 16,086 KP available in

550 Pathogenwatch together with available metadata and genotyping data (Argimon et al.,

551 2021) (https://pathogen.watch/genomes/all?genusId=570&speciesId=573) (**Table S2**).

552

553 Phylogenetic analysis of the ST258/512 collection

554 To generate a phylogenetic tree of the ST258/512 collection, we first used the

555 "to_perfect_reads" function within Fastaq v3.17.0 (https://github.com/sanger-

556 pathogens/Fastaq) to generate pseudo sequence reads for isolates where only an

557 assembly was available. We then mapped all sequence reads to the reference genome,

558 NJST258_1 (accession CP006923) (Deleo et al., 2014), using Burrows Wheeler Aligner

559 v0.7.17 (Li & Durbin, 2009). A pipeline comprising SAMtools mpileup v0.1.19 (Li et al.,

560 2009) and BCFtools v0.1.19 was used to call SNPs and generate a pseudo-genome

561 alignment. Gubbins v2.4.1 (Croucher et al., 2015) was used to remove recombined

562 regions from the alignment and generate a maximum likelihood tree with the remaining

563 variable positions. The phylogenetic tree was rooted using an outgroup isolate from a

564 closely-related ST, ST895 (accession SRR5385992), which was later removed from the

565 tree.

566 Identification and characterisation of *ompK35 and ompK36* genes

567 The *ompK35 and ompK36* genes were identified in all short-read assemblies by

568 performing BLASTn v2.6.0 (Altschul et al., 1990) with a query gene from the reference

569 genome, ATCC43816 (the parental strain of ICC8001 (Wong et al., 2019)) (accession

570 CP009208). We required a single hit of each gene per genome that matched ≥10% of the

571 query length, possessed ≥90% nucleotide similarity and contained a start codon in order

572 to unambiguously identify the gene. Nucleotide sequences were translated to protein

573 sequences in Seaview v4.7 (Gouy et al., 2010) using the standard genetic code, and the

574 protein lengths were determined. Protein sequences were predicted to be intact if they

575 contained a signal sequence, a L3 sequence and sixteen beta-barrel sequences, as

576 determined using BLASTx v2.6.0 (Gish & States, 1993). Intact protein sequences of each

577 porin were aligned using MUSCLE v3.8 (Edgar, 2004) and the different variants present

578 were identified, taking into account all amino acid substitutions, insertions and deletions.

579 Analysis of *ompK36* variation

580 The alignment of intact *ompK36* nucleotide sequences from the ST258/512 collection was

581 curated manually to ensure accurate positioning of bases around the L3 region (some of

582 which were misaligned due to indels). We then used the sequences from the curated

583 alignment to infer the likely base harboured by each internal node of the ST258/512

584 phylogenetic tree at each position in *ompK36*. This ancestral reconstruction was

585 performed with PastML v1.9.30 (Ishikawa et al., 2019) using maximum parsimony with

586 the accelerated transformation (ACCTRAN) model. Using the predicted states of all

587 internal nodes and the known bases in all terminal nodes, we determined the total number

588 of changes at each position that had occurred across the ST258/512 tree.

589 <u>Codon usage</u>

590 The frequency of different leucine codons was determined across all protein-coding

591 genes in the ATCC43816 reference genome, as well as all annotated assemblies in the

592 ST258/512 collection, using the EMBOSS v6.6.0.0 "cusp" tool

593 (http://emboss.sourceforge.net/apps/release/6.3/emboss/apps/cusp.html).

594 <u>5' untranslated region analysis</u>

595 The 500bp upstream region of *ompK36* was analysed and annotated in Fig. 4D using

596 BPROM (Solovyez & Salamov, 2011). The SDS was identified manually by consensus

597 with other KP genes.

598 <u>General cloning, molecular biology and strain generation</u>

599 All *in vitro* assays and animal infections with KP were carried out using ICC8001, a strain

600 derived by animal passage from ATCC43816 (Wong et al., 2019).

601 A homologous recombination technique resulting in scarless markerless mutants was

602 used to generate all strains based on the Standard European Vector Architecture platform

603 pSEVA612S (JX560380.2) mutagenesis plasmid. Briefly, mutants were generated in two

604 sequential recombination steps. The first step integrates the mutagenesis plasmid into

605 the genome  generating a merodiploid. The mutagenic plasmid was introduced by three

606 part conjugation and homologous recombination promoted by lambda-recombinase

607 expressed from a helper plasmid. The second step induces double strand DNA breaks

608 by induction (L-arabinose) of I-SceI expression from the helper plasmid. Double stranded

609  breaks are induced at I-SceI sites located on the chromosomally integrated mutagenesis

610  vector, flanking the final integration region. This technique has been used to efficiently

611  recombineer in KP (Wong et al., 2019) and other *Enterobacteriaceae* (Berger et al., 2017)

612  as described in respective manuscripts.

613  Mutagenesis vectors were generated by routine molecular biological techniques. These

614  included plasmid preparation (Monarch Plasmid Miniprep Kit, NEB), genomic DNA

615  extraction from bacterial cells (DNEasy, QIAGEN), polymerase chain reaction (Q5 High-

616  Fidelity 2x Master Mix and OneTaq, Quick-Load 2X Master Mix, both NEB), PCR clean-

617  up (Monarch PCR and DNA Cleanup Kit, NEB) and gel extraction (Monarch Gel

618  Extraction Kit, NEB), site directed mutagenesis (KLD enzyme blend, NEB) and Gibson

619  assembly (Gibson Assembly Master Mix, NEB). Sanger sequencing was carried out to

620  check vector construction and seamless integration into the genome (Eurofins

621  Genomics). Custom primers in this study were made by Sigma-Aldrich.

622  *ompK35* mutagenesis

623  *ompK35* wild-type ORF (+500bp flanking regions) was cloned from ICC8001 genomic

624  DNA with primers (P) 1/P2 and ligated by Gibson Assembly into pSEVA612S, linearised

625  with P3/P4. The ORF was removed by inverse PCR to generate the genomic deletion

626  vector (P5/P6) and plasmid recircularized from PCR product (KLD enzyme blend, NEB).

627  *ompK36* mutagenesis

628  ICC8001Δ*ompK36* was generated in previous work (Vector 5 in Wong et al., 2019).

629  *ompK36* wild-type ORF (+500bp flanking regions) was cloned from ICC8001 genomic

630  DNA with primers P7/P8 and ligated by Gibson assembly into pSEVA612S, linearised

631  with P3/P4. In screening colonies by Sanger Sequencing we found the 25c>t mutation

632  and this was not generated by site directed mutagenesis.

### sfGFP vectors and -14a>t vectors

*Leucine 9 CTG-sfGFP (wild-type) and Leucine 9 TTG-sfGFP (25c>t transition).* The wild-type and 25c>t Sec signal sequences were cloned from the *ompK36* vectors generated above with P9/P10. sfGFP was amplified from our previously published glmS site insertion vector (Vector 13 in Wong et al., 2019) with P11/P12 and chimeric fusion generated in the mutagenesis vector ligated by Gibson Assembly.

Leucine 8 CTG-sfGFP and Leucine 8 TTG-sfGFP were generated by site-directed mutagenesis using P13/P14 and P15/P16 respectively using the Leucine 9 CTG-sfGFP (wild-type) as the template.

*5' untranslated region mutagenesis of Leucine 9 TTG-sfGFP (25c>t transition).* Mutants were generated by site-directed mutagenesis as follows: -32(a>t) (P17/P18), -31(a>t) (P17/P19), -30(a>t) (P17/P20), -29(a>t) (P17/P21), -25(a>t) (P22/P23), -23(a>t) (P22/P24), -21(a>t) (P22/P25), -20(a>t) (P22/P26), -18(a>t) (P22/P27), -17(a>t) (P22/P28), -16(a>t) (P22/P29), -14 a>t(a>t) (P22/P30) using leucine 9 TTG sfGFP as the template. The same primer pair (P22/P30) was used to introduce the -14a>t mutation into Leucine 8 CTG-sfGFP, *ompK36WT* and *ompK36WT(25c>t)* vectors.

### Introduction of pKpQIL KPC-2 plasmid

We introduced pKpQIL KPC-2 by conjugation using an *E. coli* donor following our previously published protocol (Wong et al., 2019).

### Meropenem Minimum Inhibitory Concentrations (MIC)

The meropenem MIC of strains was assessed by broth microdilution by broth microdilution in biological triplicate according to the ISO 20776-1:2019 standard and the median value taken as the final MIC.

### Outer membrane preparations and gel electrophoresis

37

657 Outer membrane proteins were purified according to a previously described protocol with

658 several modifications (Wise et al., 2018). Saturated overnight cultures of bacteria were

659 grown in LB (10g/L NaCl) and sonification was performed at 25% amplitude for 10 bursts

660 of 15 seconds each. 10 μg of protein was separated by SDS-PAGE using 12% acrylamide

661 Mini-protean TGX precast gels (Bio-Rad, USA). Gels were stained with Coomassie

662 (Sigma-Aldrich) and imaged on a ChemiDoc XRS+ (Biorad, USA).

663 Animal work

664 8-10 week old, female, 18-20g BALB/c mice were purchased from Charles River, UK. All

665 animal work took place in the institution animal facility (Association for Assessment and

666 Accreditation of Laboratory Animal Care accredited) under the auspices of the Animals

667 (Scientific Procedures) Act 1986 (PP7392693). Work was approved locally by the

668 institutional ethics committee.

669 Housing and Randomisation

670 Upon arrival animals were independently randomized into cages of 5 animals and housed

671 for an acclimatisation period of 1 week. Mice received food and water *ad libitum* and were

672 housed in a 12hour/12hour light dark cycle. Identification of animals within groups was

673 achieved by ear notching without anaesthesia at least 24 hours in advance of procedures.

674 Intratracheal administration of inoculum and infection

675 Anaesthesia was induced by intraperitoneal injection (BD Microlance 27G 13mm needle)

676 of 80mg/kg ketamine and 0.8mg/kg medetomidine. Pre-intubation body temperature was

677 maintained by contact with a heat mat (Harvard Apparatus, U.K) and eye lubricant

678 (2.0mg/g carbomer, Alcon UK) was applied.

679 Intubation was achieved as previously described (Wong et al., 2019) by placement of a

680 21G catheter (21G IV peripheral catheter (Insyte) BD Medical) using a fibreoptic

681 intubation set (Kent Scientific) following the enclosed instructions.

682 Inoculum (dose defined in graphs) was prepared by dilution of saturated overnight

683 cultures into phosphate buffered saline (PBS) (total inoculum volume 50ul) and following

684 inspiration it was dispersed with 2 x 200ul air flushes. An aliquot of inoculum was

685 enumerated for each administration and all inoculums were ±10% of the stated figure.

686 Mice recovered at 32°C (Warm Air System, Safety Cabinet Version red, VetTech, UK)

687 until spontaneous movement and received 0.8mg/kg subcutaneous (BD Microlance 27G

688 13mm needle) atipamezole to reverse the α-agonist into the neck scruff.

689 At the experimental end-point animals were anesthetized with ketamine 100mg/kg and

690 1mg/kg medetomidine by intraperitoneal injection (BD Microlance 27G 13mm needles).

691 Following the induction of anaesthesia, blood was collected by a transdiaphragmatic

692 inferior approach cardiac puncture (BD Microlance 25G 25mm needles) and animals were

693 then humanely killed, under anaesthesia, by cervical dislocation.

694 An aliquot of blood (20ul) was taken and diluted into 180ul of hypotonic lysis solution

695 (1mM EDTA in water) for enumeration of bacterial counts. The rest was placed into a

696 microtainer (BD Microtainer for serum collection, BD Medical) and allowed to clot for 1

697 hour. This was then spun according to the manufacturer's guidance and aliquoted into

698 cryobanking tubes (Greiner Bio-One) and frozen at -80℃ until analysis.

699 Lungs were dissected out, weighed and then homogenised in gentlemacs C-tubes

700 (Miltenyi Biotec) containing 3 ml complete RPMI media (RPMI supplemented with 10%

701 heat inactivated FBS, 10 mM HEPES and 1mM Sodium Pyruvate) using a gentleMac

702 Octo dissociator (Miltenyi Biotec) using the program m_lung_1 twice.

703    Bacteria were enumerated from the lung homogenate and blood by dilution in PBS and

704    plating onto solidified LB agar containing 50ug/ml rifampicin (Merck, UK).

705    Antibiotic delivery

706    We combined the meropenem (100mg/kg) with cilastatin (100mg/kg) (Merck, UK), a renal

707    dihydropeptidase inhibitor, to reduce the *in vivo* metabolism of meropenem as the murine

708    enzyme isoform has increased activity against this carbapenem compared to human

709    enzyme. Drugs were diluted in $dH_2O$. $dH_2O$ alone was administered to vehicle control

710    animals. Doses were delivered at 6 hourly intervals as previously employed in a murine

711    carbapenemase producing KP model (Ota et al., 2020). The drug mixture was delivered

712    by intraperitoneal infection (BD Microlance 27G 13mm needles) to animals at 6 hourly

713    intervals and the iliac fossa used was alternated between doses.

714    Cytokine bead assay

715    Serum IFN-γ was assessed using a custom-made mouse panel 13-plex kit

716    (LEGENDplex, BioLegend) following the manufacturer's instructions. Cytokine levels

717    were acquired using a FACSCalibur flow cytometer (BD Biosciences), and analyses were

718    performed using LEGENDplex data analysis software (BioLegend). A biological repeat

719    was considered valid only if at least 80% of all the samples run were above the limit of

720    detection; any values below the detection limit within a repeat such as this were assumed

721    to be the lowest value detectable by the assay for statistical analysis. Values below the

722    detection limit in graphs were displayed as 1 for visualisation.

723    RNA isolation and reverse transcription quantitative PCR (RT-qPCR)

724    300 μl of an LB overnight culture of KP were treated with RNAprotect Bacteria reagent

725    (Qiagen) and centrifuged at 5000 xg for 10 min. The bacterial pellet was digested in 100

726    μl TE buffer with 15 mg/ml Lysozyme (Sigma-Aldrich) and 20 μl Proteinase K (Qiagen)

727 for 10 min according to manufacturer's guidelines. RNA was isolated using the RNeasy

728 minikit (Qiagen) following the manufacturer's instructions, and RNA concentration was

729 determined using a Nanodrop 2000 spectrophotometer (ThermoFisher Scientific). 1 μg of

730 RNA was treated with RNase-free DNase (Sigma-Aldrich) for 1 h at 37 °C and cDNA was

731 then synthesized using a Moloney murine leukemia virus (MMLV) reverse transcription

732 kit with random primers following the manufacturer´s protocol (Promega). To check for

733 the presence of remaining DNA, a reaction mixture without the MMLV reverse

734 transcriptase was also included (NRT). qPCR was performed using the Power Up SYBR

735 Green master mix (ThermoFisher Scientific) and the following primers 31/32 (*ompK36*)

736 and 33/34 (*rpoB*). The assay was run on a StepOnePlus System (Applied Biosystems)

737 and results were analysed using the StepOne software (Applied Biosystems). Relative

738 gene expression levels were analyzed by using the $2^{-\Delta CT}$ (where $C_T$ is threshold cycle)

739 method.

740 <u>IVIS sfGFP fluorescence measurement</u>

741 Saturated overnight cultures of strains were diluted 1:2000 in PBS. 20ul of suspension

742 was plated onto an agar plate and allowed to dry. Following overnight incubation (16

743 hours exactly) plates were removed and imaged on an IVIS Spectrum CT imaging

744 platform (1 second exposure, Ex 465nm/Em520nm). Fluorescence over the area of the

745 spot was quantified using Living Image Software v5.4.3 (Perkin Elmer).

746 <u>Determination of RNA structures using DMS-MaPseq</u>

747 RNA structures of *ompK36*WT, *ompK36*WT(25c>t) and *ompK36*WT(24&25c>t) were determined

748 using DMS-MaPseq similarly to as described previously (Zubradt et al., 2017). The

749 principle of this method is that DMS adds methyl groups to the Watson-Crick faces of

750  unpaired adenines and cytosines in the RNA. These methyl adducts are detected during

751  reverse transcription using the TGIRT-III reverse transcriptase, which incorporates

752  random mutations in the complementary cDNA at the corresponding nucleotides. These

753  cDNA molecules are then amplified by PCR, followed by massively parallel sequencing.

754  Mutations observed on a single DNA molecule correspond to the DMS-reactive bases on

755  the parent RNA molecule if background levels of DMS-MaPseq can be observed to be

756  negligible in untreated samples. *In vitro* (*ompK36*$_{WT}$, *ompK36*$_{WT(25c>t)}$ *and*

757  *ompK36*$_{WT(24\&25c>t)}$) and *in vivo* (*ompK36*$_{WT}$ and *ompK36*$_{WT(25c>t)}$) DMS modification were

758  performed as described below to solve the RNA structures.

759  *In vitro DMS modification.* Plasmids encoding the wildtype and *ompK36* mutants were

760  isolated using miniprep (Zymo) and amplified by PCR using a forward primer containing

761  the                    T7                    promoter                    sequence

762  (TAATACGACTCACTATAGGAAAAGGCATATAACAAACAGAGGG) and the reverse

763  primer (AAGAGTATACCAGCGAGGTTAAACCGGAC). The PCR product was used as a

764  T7 Megascript *in vitro* transcription (ThermoFisher Scientific) template according to

765  manufacturer's instructions. Next, the RNA was purified using RNA Clean and

766  Concentrator$^{TM}$-5 (Zymo). 10μg RNA was denatured at 95°C for 1 min. Denatured RNA

767  was refolded by incubating in 340mM sodium cacodylate buffer (Electron Microscopy

768  Sciences) and 5mM MgCl$^{2+}$, such that the volume was 97.5μl, for 20 min at 37°C. Then,

769  2.5% DMS (Millipore-Sigma) was added and incubated for 4 mins at 37°C with whole

770  shaking at 800 r.p.m. on a thermomixer. Subsequently, DMS was neutralized by adding

771  60μl β-mercaptoethanol (BME) (Millipore-Sigma). The DMS-modified RNA was purified

772  using RNA Clean and Concentrator$^{TM}$-5 (Zymo) and eluted in 10μl water.

773    *In vivo DMS modification.* 500µl of exponentially growing *E. coli* were incubated with 10µl

774    DMS for 3 mins at 37°C shaking at 800 r.p.m. on a thermomixer. DMS was quenched by

775    adding 500µl 30% BME, followed by a 3 min 30% BME wash and 1x PBS wash. Then,

776    bacterial pellets were resuspended and incubated at room temperature for 5 mins in 500µl

777    RNAprotect® bacteria reagent (QIAGEN). Samples were centrifuged at 16000g for 5 mins

778    and supernatant removed. Pellets were resuspended in 100µl of 15mg/ml lysozyme

779    solution plus 20µl proteinase K and mixed by vortex for 10 seconds. Samples were

780    incubated at room temperature for 10 mins, vortexing every 2 mins for 10 seconds. Next,

781    samples were added with 350µl of buffer RLT plus BME (10µl BME for every 1ml of RLT),

782    vortex to mix. Then, 250µl of 96-100% ethanol was added to samples. RNA was extracted

783    using the RNeasy® Mini kit (QIAGEN) following manufacturer's instructions. DNA was

784    digested from 5-10µg of total RNA per sample using the TURBO DNA-free kit

785    (ThermoFisher Scientific) and purified using RNA Clean and Concentrator™-5 kit.

786    Following that, ribosomal RNAs were depleted using the Ribominus™ Transcriptome

787    Isolation kit for bacteria (ThermoFisher Scientific) following manufacturer's instructions.

788    RNA was purified using RNA Clean and Concentrator™-5 (Zymo) and eluted in 10µl

789    water.

790    *RT-PCR and sequencing of DMS-modified RNA.* To reverse transcribe, rRNA-depleted

791    total RNA or *in vitro*-transcribed RNA purified from the previous steps was added to 4µl

792    5x FS buffer, 1µl dNTP, 1µl 0.1M DTT, 1µl RNase Out, 1µl 10uM reverse primer

793    (CCTGAACGTTGTATTCCC) and 1µl TGIRT-III (Ingex). The reaction was incubated for

794    1.5h at 60°C. Then, to degrade the RNA, 1ul 4M NaOH was added and incubated for

795    3min at 95°C. The cDNA was purified in 10µl water using the Oligo Clean and

796    Concentrator™ kit (Zymo). Next, 1µl of cDNA was amplified using Advantage HF 2 DNA

797 polymerase (Takara) for 30 cycles according to the manufacturer's instructions (forward

798 primer: GGAAAAGGCATATAAC; reverse primer: CCTGAACGTTGTATTCCC). The PCR

799 product was purified using E-Gel<sup>TM</sup> SizeSelect<sup>TM</sup> II 2% agarose gel (Invitrogen). RNA-seq

800 library for 300bp insert size was constructed following the manufacturer's instructions

801 (NEBNext Ultra<sup>TM</sup> II DNA Library Prep Kit). The library was loaded on an iSeq-100

802 Sequencing flow cell with iSeq-100 High-throughput sequencing kit and the library was

803 run on iSeq-100 (paired-end run, 151 x 151 cycles).

804 <u>Data analysis and visualisation</u>

805 Metadata, including *ompK36* variation, were mapped onto a phylogenetic tree of the

806 ST258/512 collection using iTOL v5.7 (Letunic & Bork, 2021) for use in figures. An

807 interactive visualisation of this genome collection can also be accessed using Microreact

808 v157 (Argimon et al., 2016): https://microreact.org/project/1vWbaqARPRNc55n4yfdLyQ-

809 ompk36.

810 Graphs and statistical analysis was carried out in GraphPad Prism v9.0.0 for Mac

811 (GraphPad Software, San Diego, California USA, www.graphpad.com). Data were

812 analysed for normal distribution (based on D'Agostino-Pearson or Shapiro-Wilk normality

813 tests) and if not normally distributed a base 10 logarithmic transformation was applied

814 before statistical analysis. When normality was not achieved by transformation, a non-

815 parametric test was applied. Statistical tests applied for each analysis are described in

816 associated figure legends.

817 Custom images of mice in Fig. 3 were made with Biorender (created with

818 BioRender.com). Images were edited and compiled into figures in Affinity Designer

819 v1.8.4. (Serif Europe Ltd).

820

821     <u>Primers</u>

822     P1 GCCAGTATAGGGATAACAGGGTAATCCGGTACCGCCCGGTGTCTG

823     P2 CGCCGGATTACCCTGTTATCCCTAGGAAATCACAATTATGTTACG

824     P3 ATTACCCTGTTATCCCTATAC

825     P4 TAGGGATAACAGGGTAATCCG

826     P5 TCTGCAGTACACCCCTTC

827     P6 CATTATTTATTACCCTC

828     P7 GATTACGCCGGATTACCCTGTTATCCCTAGGCCTAATTGATTGATTAATAG

829     P8 GGCCAGTATAGGGATAACAGGGTAATAGCCCCACAGGTTGACCAGC

830     P9 GTTGCAAGCTGCATAAC

831     P10 CGCATTTGCTGCGCCTGCTAC

832     P11 GTAGCAGGCGCAGCAAATGCGCGTAAAGGCGAAGAGCTG

833     P12 GTTATGCAGCTTGCAACCGCGAAGTAATCTTTTCG

834     P13 TTAACTTTCATGTTATTAACCCTCTGTTTGTTATATG

835     P14 AGTACTGTCCCTGCTGGTACCGG

836     P15 AGTACTGTCCTTGCTGGTACCGG

837     P16 TTAACTTTCATGTTATTAACCCTCTG

838     P17 GCATATAACAAACAGAGGGTTAATAAC

839     P18 CTTTAATTATGCCACTGC

840     P19 CTTATATTATGCCACTGC

841     P20 CTATTATTATGCCACTGC

842     P21 CATTTATTATGCCACTGC

843     P22 CTTTTATTATGCCACTGC

844     P23 GCTTATAACAAACAGAGGGTTAATAAC

845    P24 GCATTTAACAAACAGAGGGTTAATAAC

846    P25 GCATATTACAAACAGAGGGTTAATAAC

847    P26 GCATATATCAAACAGAGGGTTAATAAC

848    P27 GCATATAACTAACAGAGGGTTAATAAC

849    P28 GCATATAACATACAGAGGGTTAATAAC

850    P29 GCATATAACAATCAGAGGGTTAATAAC

851    P30 GCATATAACAAACTGAGGGTTAATAAC

852    P31 CCAGACCTACAACGCAACT

853    P32 CGCTCCAGATCCTTACCTTTAG

854    P33 AAGGCGAATCCAGCTTGTTCAGC

855    P34 TGACGTTGCATGTTCGCACCCATCA

856

857    <u>Data availability</u>

858    Raw sequence data or assemblies from the extended ST258/512 collection were

859    published in multiple manuscripts and obtained from the European Nucleotide Archive

860    (ENA). Genome assemblies from the larger KP collection were obtained from

861    Pathogenwatch (https://pathogen.watch/genomes/all?genusId=570&speciesId=573). A

862    full list of accession numbers for all data is available in Tables S1 and S2.

863

864    **References**

865    Achouak, W., Heulin, T. and Pagès, J. M. (2001). Multiple facets of bacterial porins.

866    FEMS Microbiol Lett *199*(1), 1-7.

867    Adler, A., Lifshitz, Z., Gordon, M., Ben-David, D., Khabra, E., Masarwa, S., Zion, O.,

868    Schwaber, M. J. and Carmeli, Y. (2017). Evolution and dissemination of the Klebsiella

pneumoniae clonal group 258 throughout Israeli post-acute care hospitals, 2008-13. J Antimicrob Chemother *72*(8), 2219-2224.

Altschul, S. F., Gish, W., Miller, W., Myers, E. W. and Lipman, D. J. (1990). Basic local alignment search tool. J Mol Biol *215*(3), 403-10.

Argimón, S., Abudahab, K., Goater, R. J. E., Fedosejev, A., Bhai, J., Glasner, C., Feil, E. J., Holden, M. T. G., Yeats, C. A., Grundmann, H., Spratt, B. G. and Aanensen, D. M. (2016). Microreact: visualizing and sharing data for genomic epidemiology and phylogeography. Microb Genom *2*(11), e000093.

Argimón, S., David S., Underwood, A., Abrudan A., Wheeler, NE., Kekre, M., Abudahab, K., Yeats, C. A., Goater, R., Taylor, B., Harste, H., Muddyman, D., Feil, E. J., Brisse, S., Holt, K., Gonado-Godoy, P., Ravikumar, K. L., Okeke, I. N., Carlos, C., Aanensen, D. M. (2021). Rapid Genomic Characterisation and Global Surveillance of Klebsiella using Pathogenwatch. bioRxiv. https://doi.org/10.1101/2021.06.22.448967

Bajaj, H., Scorciapino, M. A., Moynié, L., Page, M. G., Naismith, J. H., Ceccarelli, M. and Winterhalter, M. (2016). Molecular Basis of Filtering Carbapenems by Porins from β-Lactam-resistant Clinical Strains of Escherichia coli. J Biol Chem *291*(6), 2837-47.

Bankevich, A., Nurk, S., Antipov, D., Gurevich, A. A., Dvorkin, M., Kulikov, A. S., Lesin, V. M., Nikolenko, S. I., Pham, S., Prjibelski, A. D., Pyshkin, A. V., Sirotkin, A. V., Vyahhi, N., Tesler, G., Alekseyev, M. A. and Pevzner, P. A. (2012). SPAdes: a new genome assembly algorithm and its applications to single-cell sequencing. J Comput Biol *19*(5), 455-77.

Berger, C. N., Crepin, V. F., Roumeliotis, T. I., Wright, J. C., Carson, D., Pevsner-Fischer, M., Furniss, R. C. D., Dougan, G., Dori-Bachash, M., Yu, L., Clements, A., Collins, J. W., Elinav, E., Larrouy-Maumus, G. J., Choudhary, J. S. and Frankel, G. (2017). Citrobacter rodentium Subverts ATP Flux and Cholesterol Homeostasis in Intestinal Epithelial Cells In Vivo. Cell Metab *26*(5), 738-752.e6.

Bhattacharyya, S., Jacobs, W. M., Adkar, B. V., Yan, J., Zhang, W. and Shakhnovich, E. I. (2018). Accessibility of the Shine-Dalgarno Sequence Dictates N-Terminal Codon Bias in E. coli. Mol Cell *70*(5), 894-905.e5.

Bowers, J. R., Kitchel, B., Driebe, E. M., MacCannell, D. R., Roe, C., Lemmer, D., de Man, T., Rasheed, J. K., Engelthaler, D. M., Keim, P. and Limbago, B. M. (2015).

Genomic Analysis of the Emergence and Rapid Global Dissemination of the Clonal Group 258 Klebsiella pneumoniae Pandemic. Plos One *10*(7).

Cassini, A., Högberg, L. D., Plachouras, D., Quattrocchi, A., Hoxha, A., Simonsen, G. S., Colomb-Cotinat, M., Kretzschmar, M. E., Devleesschauwer, B., Cecchini, M., Ouakrim, D. A., Oliveira, T. C., Struelens, M. J., Suetens, C., Monnet, D. L. (2019). Attributable deaths and disability-adjusted life-years caused by infections with antibiotic-resistant bacteria in the EU and the European Economic Area in 2015: a population-level modelling analysis. Lancet Infect Dis *19*(1), 56-66.

Chiang, M. K., Lu, M. C., Liu, L. C., Lin, C. T. and Lai, Y. C. (2011). Impact of Hfq on global gene expression and virulence in Klebsiella pneumoniae. PLoS One *6*(7) e22248.

Clancy, C. J., Chen, L., Hong, J. H., Cheng, S., Hao, B., Shields, R. K., Farrell, A. N., Doi, Y., Zhao, Y., Perlin, D. S., Kreiswirth, B. N. and Nguyen, M. H. (2013). Mutations of the ompK36 porin gene and promoter impact responses of sequence type 258, KPC-2-producing Klebsiella pneumoniae strains to doripenem and doripenem-colistin. Antimicrob Agents Chemother *57*(11), 5258-65.

Croucher, N. J., Page, A. J., Connor, T. R., Delaney, A. J., Keane, J. A., Bentley, S. D., Parkhill, J. and Harris, S. R. (2015). Rapid phylogenetic analysis of large samples of recombinant bacterial whole genome sequences using Gubbins. Nucleic Acids Res *43*(3), e15.

David, S., Reuter, S., Harris, S. R., Glasner, C., Feltwell, T., Argimon, S., Abudahab, K., Goater, R., Giani, T., Errico, G., Aspbury, M., Sjunnebo, S., Feil, E. J., Rossolini, G. M., Aanensen, D. M., and Grundmann, H. (2019). Epidemic of carbapenem-resistant Klebsiella pneumoniae in Europe is driven by nosocomial spread. Nat Microbiol *4*(11), 1919-1929.

Deleo, F. R., Chen, L., Porcella, S. F., Martens, C. A., Kobayashi, S. D., Porter, A. R., Chavda, K. D., Jacobs, M. R., Mathema, B., Olsen, R. J., Bonomo, R. A., Musser, J. M. and Kreiswirth, B. N. (2014). Molecular dissection of the evolution of carbapenem-resistant multilocus sequence type 258 Klebsiella pneumoniae. Proc Natl Acad Sci U S A *111*(13), 4988-93.

Dulyayangkul, P., Wan Nur Ismah, W. A. K., Douglas, E. J. A. and Avison, M. B. (2020). Mutation of *kvrA* Causes OmpK35 and OmpK36 Porin Downregulation and Reduced

Meropenem-Vaborbactam Susceptibility in KPC-Producing Klebsiella pneumoniae. Antimicrob Agents Chemother *64*(7).

Dé, E., Baslé, A., Jaquinod, M., Saint, N., Malléa, M., Molle, G. and Pagès, J. M. (2001). A new mechanism of antibiotic resistance in Enterobacteriaceae induced by a structural modification of the major porin. Mol Microbiol *41*(1), 189-98.

Edgar, R. C. (2004). MUSCLE: a multiple sequence alignment method with reduced time and space complexity. BMC Bioinformatics *5*, 113.

Elliott, E., Brink, A. J., van Greune, J., Els, Z., Woodford, N., Turton, J., Warner, M. and Livermore, D. M. (2006). In vivo development of ertapenem resistance in a patient with pneumonia caused by Klebsiella pneumoniae with an extended-spectrum beta-lactamase. Clin Infect Dis *42*(11), e95-8.

EUCAST guidelines. (2021). https://www.eucast.org/clinical_breakpoints/

Fajardo-Lubián, A., Ben Zakour, N. L., Agyekum, A., Qi, Q. and Iredell, J. R. (2019). Host adaptation and convergent evolution increases antibiotic resistance without loss of virulence in a major human pathogen. PLoS Pathog *15*(3), e1007218.

Giakkoupi, P., Papagiannitsis, C. C., Miriagou, V., Pappa, O., Polemis, M., Tryfinopoulou, K., Tzouvelekis, L. S. and Vatopoulos, A. C. (2011). An update of the evolving epidemic of blaKPC-2-carrying Klebsiella pneumoniae in Greece (2009-10). J Antimicrob Chemother 66(7), 1510-3.

Giani, T., Pini, B., Arena, F., Conte, V., Bracco, S., Migliavacca, R., Pantosti, A., Pagani, L., Luzzaro, F., Rossolini, G. M. and Participants, A.-C. S. (2013). Epidemic diffusion of KPC carbapenemase-producing Klebsiella pneumoniae in Italy: results of the first countrywide survey, 15 May to 30 June 2011. Euro Surveill *18*(22).

Gish, W. and States, D. J. (1993). Identification of protein coding regions by database similarity search. Nat Genet *3*(3), 266-72.

Gouy, M., Guindon, S. and Gascuel, O. (2010). SeaView version 4: A multiplatform graphical user interface for sequence alignment and phylogenetic tree building. Mol Biol Evol *27*(2), 221-4.

Ishikawa, S. A., Zhukova, A., Iwasaki, W. and Gascuel, O. (2019). A Fast Likelihood Method to Reconstruct and Visualize Ancestral Scenarios. Mol Biol Evol *36*(9), 2069-2085.

963   Kitchel, B., Rasheed, J. K., Patel, J. B., Srinivasan, A., Navon-Venezia, S., Carmeli, Y.,

964   Brolund, A. and Giske, C. G. (2009). Molecular epidemiology of KPC-producing

965   Klebsiella pneumoniae isolates in the United States: clonal expansion of multilocus

966   sequence type 258. Antimicrob Agents Chemother *53*(8), 3365-70.

967   Kohira, N., West, J., Ito, A., Ito-Horiyama, T., Nakamura, R., Sato, T., Rittenhouse, S.,

968   Tsuji, M. and Yamano, Y. (2016). In Vitro Antimicrobial Activity of a Siderophore

969   Cephalosporin, S-649266, against Enterobacteriaceae Clinical Isolates, Including

970   Carbapenem-Resistant Strains. Antimicrob Agents Chemother *60*(2), 729-34.

971   Kudla, G., Murray, A. W., Tollervey, D. and Plotkin, J. B. (2009). Coding-sequence

972   determinants of gene expression in Escherichia coli.  Science *324*(5924), 255-8.

973   Lam, M. M. C., Wick, R. R., Watts, S. C., Cerdeira, L. T., Wyres, K. L. and Holt, K. E.

974   (2021). A genomic surveillance framework and genotyping tool for Klebsiella

975   pneumoniae and its related species complex. Nat Commun *12*(1), 4188.

976   Letunic, I. and Bork, P. (2021). Interactive Tree Of Life (iTOL) v5: an online tool for

977   phylogenetic tree display and annotation. Nucleic Acids Res *49*(W1), W293-W296.

978   Li, H. and Durbin, R. (2009). Fast and accurate short read alignment with Burrows-

979   Wheeler transform. Bioinformatics *25*(14), 1754-60.

980   Li, H., Handsaker, B., Wysoker, A., Fennell, T., Ruan, J., Homer, N., Marth, G.,

981   Abecasis, G., and Durbin, R. (2009). The Sequence Alignment/Map format and

982   SAMtools. Bioinformatics *25*(16), 2078-2079.

983   Lister, P. D., Wolter, D. J. and Hanson, N. D. (2009). Antibacterial-resistant

984   Pseudomonas aeruginosa: clinical impact and complex regulation of chromosomally

985   encoded resistance mechanisms. Clin Microbiol Rev *22*(4), 582-610.

986   Moore, T. A., Perry, M. L., Getsoian, A. G., Newstead, M. W. and Standiford, T. J.

987   (2002). Divergent role of gamma interferon in a murine model of pulmonary versus

988   systemic Klebsiella pneumoniae infection. Infect Immun *70*(11), 6310-8.

989   Ota, K., Kaku, N. and Yanagihara, K. (2020). Efficacy of meropenem and amikacin

990   combination therapy against carbapenemase-producing Klebsiella pneumoniae mouse

991   model of pneumonia. J Infect Chemother *26*(12), 1237-1243.

992   Roberts, J. A., Paul, S. K., Akova, M., Bassetti, M., De Waele, J. J., Dimopoulos, G.,

993   Kaukonen, K. M., Koulenti, D., Martin, C., Montravers, P., Rello, J., Rhodes, A., Starr,

994   T., Wallis, S. C., and Lipman, J. (2014). DALI: defining antibiotic levels in intensive care

995     unit patients: are current β-lactam antibiotic doses sufficient for critically ill patients? Clin
996     Infect Dis *58*(8), 1072-83.

997     Rojas, L. J., Weinstock, G. M., De La Cadena, E., Diaz, L., Rios, R., Hanson, B. M.,
998     Brown, J. S., Vats, P., Phillips, D. S., Nguyen, H., Hujer, K. M., Correa, A., Adams, M.
999     D., Perez, F., Sodergren, E., Narechania, A., Planet, P. J., Villegas, M. V., Bonomo, R.
1000     A. and Arias, C. A. (2017). An Analysis of the Epidemic of Klebsiella pneumoniae
1001     Carbapenemase-Producing K. pneumoniae: Convergence of Two Evolutionary
1002     Mechanisms Creates the "Perfect Storm". J Infect Dis *217*(1), 82-92.

1003     Seemann, T. (2014). Prokka: rapid prokaryotic genome annotation. Bioinformatics
1004     *30*(14), 2068-9.

1005     Solovyez, V. and Salamov, A. (2011). Metagenomics and its Applications in Agriculture,
1006     Biomedicine and Environmental Studies (Nova Sciences Publishers).

1007     Tran, Q. T., Mahendran, K. R., Hajjar, E., Ceccarelli, M., Davin-Regli, A., Winterhalter,
1008     M., Weingart, H. and Pagès, J. M. (2010). Implication of porins in beta-lactam
1009     resistance of Providencia stuartii. J Biol Chem *285*(42), 32273-81.

1010     Tsai, Y. K., Fung, C. P., Lin, J. C., Chen, J. H., Chang, F. Y., Chen, T. L. and Siu, L. K.
1011     (2011). Klebsiella pneumoniae outer membrane porins OmpK35 and OmpK36 play
1012     roles in both antimicrobial resistance and virulence. Antimicrob Agents Chemother
1013     55(4), 1485-93.

1014     Vergalli, J., Bodrenko, I. V., Masi, M., Moynié, L., Acosta-Gutiérrez, S., Naismith, J. H.,
1015     Davin-Regli, A., Ceccarelli, M., van den Berg, B., Winterhalter, M. and Pagès, J. M.
1016     (2020). Porins and small-molecule translocation across the outer membrane of Gram-
1017     negative bacteria. Nat Rev Microbiol *18*(3), 164-176.

1018     Vincent, J. L., Sakr, Y., Singer, M., Martin-Loeches, I., Machado, F. R., Marshall, J. C.,
1019     Finfer, S., Pelosi, P., Brazzi, L., Aditianingsih, D., Timsit, J. F., Du, B., Wittebole, X.,
1020     Máca, J., Kannan, S., Gorordo-Delsol, L. A., De Waele, J. J., Mehta, Y., Bonten, M. J.
1021     M., Khanna, A. K., Kollef, M., Human, M., and Angus, D. C. (2020). Prevalence and
1022     Outcomes of Infection Among Patients in Intensive Care Units in 2017. JAMA *323*(15),
1023     1478-1487.

1024     Wise, M. G., Horvath, E., Young, K., Sahm, D. F. and Kazmierczak, K. M. (2018).
1025     Global survey of Klebsiella pneumoniae major porins from ertapenem non-susceptible
1026     isolates lacking carbapenemases. J Med Microbiol *67*(3), 289-295.

1027  Wong, J. L. C., Romano, M., Kerry, L. E., Kwong, H. S., Low, W. W., Brett, S. J.,

1028  Clements, A., Beis, K. and Frankel, G. (2019). OmpK36-mediated Carbapenem

1029  resistance attenuates ST258 Klebsiella pneumoniae in vivo. Nat Commun *10*(1), 3957.

1030  Yoshida, K., Matsumoto, T., Tateda, K., Uchida, K., Tsujimoto, S., Iwakura, Y. and

1031  Yamaguchi, K. (2001). Protection against pulmonary infection with Klebsiella

1032  pneumoniae in mice by interferon-gamma through activation of phagocytic cells and

1033  stimulation of production of other cytokines. J Med Microbiol *50*(11), 959-964.

1034  Yoshino, M., Aihara, M., Gotoh, Y., Akimoto, M., Tatsuhara, W., Kiyosuke, M.,

1035  Matsushima, Y., Uchiumi, T., Hayashi, T. and Kang, D. (2021). Stepwise Evolution of a

1036  Klebsiella pneumoniae Clone within a Host Leading to Increased Multidrug Resistance.

1037  mSphere e0073421.

1038  Zubradt, M., Gupta, P., Persad, S., Lambowitz, A. M., Weissman, J. S. and Rouskin, S.

1039  (2017). DMS-MaPseq for genome-wide or targeted RNA structure probing in vivo. Nat

1040  Methods *14*(1), 75-82.